Stratigraphy of Architectural Elements of a Buried Monogenetic Volcanic System and Implications for Geoenergy Exploration

Alan Bischoff [a]*, Andy Nicol [a], Jim Cole [a], Darren Gravley [a]

a Department of Geological Sciences, University of Canterbury, Christchurch, New Zealand;

alan.bischoff@canterbury.ac.nz

 *corresponding author

Stratigraphy of Architectural Elements of a Buried Monogenetic Volcanic System and Implications for Geoenergy Exploration

Large volumes of magma emplaced and deposited within sedimentary basins can have an impact on their architectural style and geological evolution. Over the last decade, continuous improvement in techniques such as seismic volcano-stratigraphy and 3D seismic visualization of igneous rocks buried in sedimentary basins has helped increase knowledge about these "volcanic basins". Here, we unravel the complete architecture of the Maahunui Volcanic System (MVS), a middle Miocene monogenetic volcanic field now buried in the offshore Canterbury Basin, South Island of New Zealand. We show the location, geometry, size, and stratigraphic relationships between 25 main intrusive, eruptive, and sedimentary architectural elements in a comprehensive volcano-stratigraphic framework that explains the evolution of the MVS from emplacement to complete burial. The plumbing system of the MVS comprises of seven main architectural elements, including saucer-shaped sills, dikes and sills swarms, minor stocks and laccoliths, and pre-eruptive strata deformed by intrusions. These endogenous elements occur in five distinctive plumbing-types, controlled by the emplacement depth, and by the geometric relationships between the intrusions and the enclosing strata. The exogenous volcanic architecture is defined by a combination of eruptive and associated sedimentary architectural elements, with minor and localized shallow intrusions. Characteristic volcano-types of the MVS are interpreted as the deep-water equivalents of crater and cone-type volcanoes. Crater-type volcanoes have eight main architectural elements (i.e. root zone, lower and upper diatreme, tephra ring, tephra plain, intra-crater cones, overspill wedge and tephra fallow carpet). Cone-type volcanoes have five main architectural elements (i.e. basal cone, central crater, tephra flank, cone apron and tephra fallout carpet). After volcanism has ceased, the process of degradation and burial of the volcanic edifices produces five main sedimentary architectural elements (i.e. inter-cone plains, epiclastic plumes, canyons and gullies, burial domes and seamount-edge fans). Understanding the relationships between these diverse architectural elements allow us to reconstruct the complete architecture of the MVS, and to recognize the main volcano-stratigraphic trends in the study area. The characterisation of architectural elements of the MVS can be applied to explore opportunities to find valuable geoenergy resources such as oil, gas and geothermal energy with buried and active monogenetic volcanic systems.

Keywords: buried volcanoes; monogenetic field; seismic reflection; geoenergy.

Introduction

Volcanoes buried in sedimentary basins can form very complex magmatic-sedimentary systems (e.g. Planke et al., 1999; Holford et al., 2012; Schofield et al., 2012; Bischoff et al., 2017; Morley, 2018). The large-scale architecture of buried volcanoes can be broadly divided into two realms. In the endogenous realm, magma emplaced within sedimentary strata can form a great variety of intrusive bodies, each with different morphologies, sizes and contact relationships with the host rocks, which is typically controlled by the equilibrium of magma pressure vs. lithostatic pressure (e.g. Lister et al., 1991; Rubin, 1995; O'Neill et al., 2010; apud Kereszturi and Németh, 2013). In contrast, magma that reaches the Earths' surface (exogenous realm) typically produces diverse terrestrial and submarine morphologies, which is largely defined by the interplay between magma composition, eruptive styles, edifice growth mechanisms, interaction with external environments, and tectonic settings (e.g. Cas and Wright, 1993; Kereszturi et al, 2011; Silva and Lindsay, 2015; Rogers, 2015; Planke et al., 2017).

The great number of intrusive, eruptive and sedimentary bodies present in buried volcanoes can complicate their architectural characterisation. Studies that describe the morphology (i.e. the form) and architecture (i.e. the arrangement of the parts) of monogenetic volcanoes are well constrained from the interpretation of modern and ancient outcropping systems (e.g. Lorenz, 1985; Cas and Wright, 1993; Orton, 1996; Kereszturi et al., 2010; Németh, 2010; Kereszturi and Németh, 2013; Silva and Lindsay, 2015). However, complete architectural characterisation based in outcrops observation of both endogenous and exogenous parts of monogenetic fields is only possible in rare exhumed volcanic fields (e.g. White, 1991; Muirhead et al., 2016). Because of this, significant research remains necessary to understand the key processes that control volcanic and sub-volcanic architecture together. High-quality 2D and 3D seismic surveys can provide a valuable opportunity to observe buried volcanic systems on scales ranging from seismic to outcrop analogues (e.g. Jerram et al., 2009; Schofield et al., 2012; Planke et al., 2017; Rabbel et

al., 2018). This approach can be enriched by coupling the seismic data with information from borehole samples, wireline data, and laboratory experiments (e.g. Planke et al., 1999; Millett et al., 2015). Currently, very few studies have been conducted to characterise the architecture of monogenetic volcanic systems from their emplacement to complete burial (e.g. Reynolds et al, 2016; McLean et al., 2017). Here, we adapt the approach presented in Bischoff et al. (2017) for polygenetic volcanic systems, to describe the complete architecture of the Maahunui Volcanic System (MVS), a submarine monogenetic volcanic field currently buried by ca 1000 m in the offshore Canterbury Basin, New Zealand (Bischoff, 2019). Interpretation of the "big picture" of buried volcanic systems can provide valuable insights into how they evolve in time and space, especially if these "fossilized" systems are compared with modern outcropping analogues (Planke et al., 2017; Gallant et al., 2018). Understanding the complete architecture of volcanic systems is beneficial for estimating their potential to host geoenergy resources such as petroleum and geothermal energy in association with buried and modern volcanoes.

Geological Background

The Maahunui Volcanic System (MVS) comprise a cluster of at least 31 middle Miocene small-volume (<6 km^3) volcanoes currently buried by ca 1000 m in sedimentary strata of the Canterbury Basin, New Zealand (Bischoff, 2019). Volcanism occurred semi-continuously during the geological evolution of Canterbury Basin (Suggate et al., 1978; Field et al., 1989; Barrier et al., 2017). During the Cenozoic, the Canterbury Basin experienced widespread and long-lived intraplate volcanism (Finn et al., 2005; Timm et al., 2010). Products of this magmatism are primarily mafic in composition and formed both monogenetic volcanic fields such as the Waiareka/Deborah and Waipiata Volcanic Fields (e.g. Coombs et al., 1986; Németh and White, 2003), and large polygenetic volcanic complexes like those from Banks and Otago Peninsulas (e.g. Coombs et al., 1960; Sewell, 1988). In the offshore Canterbury Basin, several late Cretaceous to Pleistocene buried volcanoes and intrusive bodies have been mapped using

seismic reflection data (Field et al., 1989; Blanke, 2012; Bischoff, 2016; Barrier et al., submitted). However, despite a dozen of exploration boreholes have recovered representative rocks of these buried volcanoes, little is known about the eruptive histories due to a lack of detailed studies.

Volcanoes of the MVS were imaged by high-quality 2D seismic lines and drilled by the petroleum exploration well Resolution-1 (Figure 1), which recovered a monzogabbro intrusion and correlative middle Miocene volcanoclastic rocks (Milne, 1975). Volcanism in the MVS is estimated to be active from 12.7 to 11.5 Ma (Bischoff, 2019). The products of this volcanic activity is mapped over an area of ca 1,520 km^2, located ca 40 km south and offshore of Banks Peninsula (Figure 1). Eruptions in the MVS were short-lived and entirely submarine (500 to 1500 m in depth), controlled by a plumbing system that fed magma to disperse eruptive centres, a characteristic of monogenetic volcanic fields (Bischoff, 2019). After volcanism ceased, volcanoes located in a bathyal setting were buried and well preserved in the Canterbury Basin sedimentary strata, while high volcanoes (> 200 m) located in a neritic setting were emergent at the paleo sea-surface and have their tops flattened by erosional processes (Bischoff, 2019).

Dataset, Methods and Concepts

In this study, we used more than 40,000 km of high-quality 2D seismic lines correlated with data from one borehole (Resolution-1) to interpret how diverse architectural elements vary in time and space in the MVS (Figure 1). We contrast the observations from this dataset with insights from tens of outcropping, submerged, and buried volcanic systems imaged by 3D seismic surveys from New Zealand sedimentary basins and elsewhere. The compiled datasets are complementary, providing information about the rock-types, eruptive styles, magma-sediment interactions, volcanic morphologies, and volcanic architecture within the basin strata. The available information helps us to build a comprehensive volcano-stratigraphic framework (Figure 2) showing the locations of individual (or sets of) cogenetic volcanic and sedimentary

architectural elements and explaining the complete architecture of the Maahunui Volcanic

System (MVS) from emplacement to burial. The *volcanic system* concept applied in this work is

an extension of the igneous boundaries of the Maahunui Volcanic Field (MVF) presented in

Bischoff (2019), and includes two extra parts: i) the sedimentary strata deformed by intrusions,

and ii) the post-eruptive sedimentary deposits impacted by the presence of the volcanoes (Figure

2), according the model of Bischoff et al. (2017).

Magmatic-stratigraphic framework of buried volcanoes

Similarly to standard methods applied to analyse the stratigraphic record of *sensu strict*

sedimentary basin analysis (e.g. Mitchum et al., 1977; Posamentier and Vail, 1988; Van

Wagoner et al., 1990; Catuneanu, 2006), the magmatic-stratigraphy framework of MVS was

built from observations of stratigraphic surfaces that represent shifts in the local architecture of

the basin. This shifts mark the boundaries between the magmatic sequences and stages in the

study area, following and extending the approach proposed in Bischoff et al., 2017. In this study,

we used a model-independent methodology to identify the bounding surfaces that mark

important shifts in basin stratal patterns (Catuneanu et al., 2009; 2010). In volcanic basins (e.g.

Rohrman, 2007; Planke et al., 2017; Svensen et al., 2017), these changes are strictly controlled

by expressive igneous events (e.g. Herzer, 1995; Planke et al., 2000; Bischoff et al., 2016; 2017;

2019). Recognition of these important magmatic signatures printed in the record of volcanic

basins encourages us to propose a magmatic-stratigraphic model based on sequences bounded by

the beginning and end of distinct magmatic stages experienced during basin evolution and

magmatic activity. We subdivide the stratigraphic record of the MVS into three first-order

stratigraphic intervals (i.e. pre, syn and post-magmatic sequences). The pre-magmatic sequence

predates magmatism and is cross-cut by the volcanic plumbing system. The syn-magmatic

sequence comprises of both intrusive and extrusive parts of the volcano. The post-magmatic

sequence is characterised by degradation and burial of the volcanic structures after magmatism

has ceased. These first-order sequences can be sub-divided into second-order magmatic stages (i.e. emplacement, construction, degradation and burial stages), according to the dominant magmatic or sedimentary processes that control the basin architecture at each time (Figure 2).

Definition of the magmatic-stratigraphic surfaces follow well-established terminology such as pre-eruptive surface (PrErS) and post-eruptive surfaces (PoErS). In other cases, we introduce new terminology such as syn-intrusive surface (SyInS), post-degradational surface (PoDgS) and post-burial surface (PoBuS). The main magmatic-stratigraphic surfaces are defined as follows. The upper stratigraphic boundary of the pre-magmatic sequence (Figure 2) is defined by the oldest (in age) eruptive event in the volcanic field, and corresponds to the PrErS. Its lower and lateral limits are defined by the SyInS, which is an arbitrary boundary that limits the occurrence of intrusive bodies and associated deformation in the study area. The syn-magmatic sequence (Figure 2) is subdivided into two magmatic stages: i) the emplacement stage has its upper boundary at the PrErS, and an arbitrary lateral limit at the SyInS, ii) the constructional stage has a basal boundary defined by the PrErS, an upper boundary defined by the PoErS, which is concordant with the youngest (in age) eruptive event in the MVS. The lateral boundary of the constructional stage is defined by the extension of eruptive and time-equivalent sedimentary deposits. The post-magmatic sequence (Figure 2) is subdivided into two recurrent magmatic stages: degradational and burial. The degradational stage has a lower stratigraphic boundary at the PoErS, and an upper boundary at the PoDgS, which is an arbitrary boundary relative to one or more eruption centres, and represent the time in when the rate of degradation exceeds the rate of burial in the field. The burial stage has a lower boundary at PoErS or PoDgS, and an upper boundary at the PoBuS, which is defined as an arbitrary surface that delimits the influence of the buried volcanic edifices on basin sedimentation. Table 1 shows the characteristics of these surfaces and their correlative magmatic sequences and stages in the MVS.

Volcanic and Sedimentary Architectural Elements

Each one of the MVS magmatic stages is characterised by a network of genetically related fundamental building blocks (i.e. architectural elements), formed by interactions between intrusions, eruptions, and sedimentation. The concept of architectural elements was introduced by Allen (1983) and extended by Miall (1985) to describe sets of genetically related rock associations that form the fundamental building blocks of fluvial systems. The application of the architectural element concept is now widely used in most clastic systems (e.g. Mutti and Normark, 1987; Miall and Tyler, 1991; Miall, 2000; Borgui 2000; Posamentier and Kolla, 2003; Slatt, 2006; Moraes et al., 2006; Gamboa and Alves, 2015), and has also been successfully applied in carbonate systems (e.g. Kendall and Tucker, 2010; Catuneanu et al., 2011; Liu et al., 2018). To our knowledge, Bischoff et al. (2017) was pioneer to apply this concept to characterise the architecture of volcanic systems.

Interpretation of the architectural elements of the MVS (Figure 3) was primarily achieved by observations from 2D seismic lines that image the volcanic field, and follows two approaches: one with complementary information from well data; the second without well data. In both approaches, we initially characterised the 2D aspects of seismic anomalies that represent buried igneous rocks in the study area, based on their morphology, internal, external and termination of seismic reflectors, geometry of enclosing strata, and surfaces that bound the anomaly from adjacent strata. Next, the results from 2D characterisation were compared with observations from outcropping and buried analogues elsewhere, searching for insights into possible 3D architectures expected to represent the seismic anomalies identified in 2D seismic data. The final output interpretation can be very similar following both approaches, however, "ground-true" confirmation of the seismic images using data from drill holes can provide an accurate geological characterisation of the anomaly, while interpretation without well data remains only hypothetical (Figure 3). Limitation of this method regards on the quality and resolution of the 2D

seismic images, which in the study area is in the order of tens of meters vertical, and maximum lateral gaps of 7 km between seismic lines.

Stratigraphy of Architectural Elements of Maahunui Volcanic System

We have identified 25 main individual architectural elements that together compose the complete architecture of MVS (Figure 4). In this section we present a detailed characterisation of each architectural element according to their stratigraphic position into the pre-, syn and post-magmatic sequences. Architectural elements formed during the pre-magmatic sequence and undeformed by magmatic processes are not described in detail further here.

-Syn Magmatic Sequence

The syn-magmatic sequence of the MVS comprises the endogenous and exogenous parts of the volcanic system. This sequence is characterised by rock units formed during the emplacement of intrusive bodies, eruptions, and time-equivalent sedimentation, as well as by pre-magmatic strata deformed by magmatic activity.

Syn-intrusive architectural elements: plumbing system and magmatic deformation

Syn-intrusive architectural elements of MVS were formed in association with the emplacement of a shallow magmatic plumbing system (up to 3 km deep) that intruded and deformed Cretaceous to middle Miocene sedimentary strata in the study area. Typically, syn-intrusive architectural elements such as sill, dikes and strata deformed by magmatism emplace within pre-magmatic sedimentary strata and occur below the PrErS surface. However, some very shallow intrusions may cross-cut or emplace within syn-eruptive deposits (Figure 4; Figure 5; Figure 6). Table 2 shows the main characteristics of the syn-intrusive architectural elements in the MVS.

MVS plumbing-types

We broadly characterise the shallow plumbing system of the MVS (up to 3 km deep) into five plumbing-types (Figure 5; Figure 6), based on the geometry, size and depth of the intrusive bodies, and on their relationship to enclosing sedimentary strata. Each plumbing-type can contains a variety of intrusive bodies such as dikes, sills and stocks, which are individually described in the latter part of this section. Figure 4, Figure 5, Figure 6 show a schematic representation and seismic images of these plumbing-types.

- Type 1: large (up to 5 km in width and ca 100 m thick) sills and saucer-shaped intrusions emplaced at deeper levels within the basin (500 to 1400 m), into Cretaceous-Paleocene sedimentary strata, showing minor branching, simple intrusive network, and extensive lateral migration of magma (up to 5 km).

- Type 2: small (up to 1 km), disrupted, parallel, transgressive or saucer-shaped intrusions emplaced into Cretaceous to Oligocene strata, showing intense lateral and vertical branching, very complex intrusive networks, and moderate magma lateral migration.

- Type 3: narrow, steeply inclined and discontinuous conduit zones, located immediately above the tips of large saucer-shaped intrusions (type-1), showing intense vertical branching, complex intrusive networks, and little lateral migration of magma.

- Type 4: shallow (up to 250 m deep) swarms of narrow, steeply inclined, parallel and transgressive intrusions, located immediately below eruptive vents, showing intense branching, complex intrusive networks, and little lateral migration of magma.

- Type 5: narrow, very deep to shallow, steeply inclined conduit zones located immediately below eruptive vents, showing little branching, simple intrusive networks, and little lateral migration of magma.

Sills and saucer-shaped sills

Sills and saucer-shaped sills are the most common syn-intrusive architectural elements in the MVS (Figure 4; Figure 5; Figure 6; Figure 8;). In the seismic data, these syn-intrusive architectural elements occur between 1.1 and 1.8 sec TWT, usually intruding paralic to marine Cretaceous-Paleocene sedimentary strata. Individual or sets of tabular, parallel, transgressive and saucer-shaped sills vary in lateral size from a few hundred meters to 5 km in width and ca 100 m in vertical dimension (Figure 6). The presence of intrusions is often associated with disrupted and deformed enclosing reflectors, demonstrating that magma transferring through the sedimentary basin can produce large scale (tens-to-hundreds of meters) structural deformation. This deformation can include folds, jacked-up strata, reverse and normal faults. These interpretations are supported by observations from sedimentary basins elsewhere (e.g. Planke et al., 2005; Hansen and Cartwright, 2006; Blanke, 2012; Holford et al., 2012; Jackson, 2012; Muirhead et al., 2016; Barrier et al., 2017; McLean et al., 2017; Schmiedel et al., 2017; Senger et al., 2017) and by laboratory experiments (Montanari et al., 2017).

Petrographic analyses (Figure 7) of a Type-1 intrusion recovered from the Resolution-1 well presented in Bischoff (2019) provides evidence that this plumbing-type has emplaced and crystalized at relatively shallow depths in the basin (ca 1000 m). Seismic images (Figure 5 and Figure 6) show a direct connection between Type-1 intrusions and many MVS eruptive vents, which in association with petrographic and geochemistry results, indicate that some of these saucer-shaped sills are likely to have fed eruptions at the middle Miocene paleo-submarine seabed (Bischoff, 2019). This relationship between the emplacement of shallow sills and eruptions was described in southern Australian (Holford et al., 2012; Reynolds et al, 2017) and North Sea sedimentary basins (Jackson, 2012; McLean et al., 2017), and also in outcrops of Hopi Buttes Volcanic Field, USA (Muirhead et al., 2016).

Dikes and magmatic conduits

Dikes and other potential magmatic conduits are syn-intrusive architectural elements characterised by vertical and sub-vertical igneous bodies emplaced beneath the pre- and post-eruptive surfaces (Figure 4; Figure 5; Figure 6). Due to their steep inclination and narrow lateral thickness, dikes and other magmatic conduits are typically seismically unresolvable. We recognize these bodies by narrow, steeply inclined, tabular high amplitude reflectors, and by sub-vertical discontinuities that crosscut pre-magmatic sedimentary strata (Figure 5; Figure 6). In the MVS, these intrusions commonly form complex branched networks, in association with sills and stocks (plumbing-types 2, 3 and 4), which is similar to networks observed from 3D seismic reflection data and wells in the Ben Nevis monogenetic volcanic field (McLean, et al., 2017). In other cases, we observe narrow sub-vertical discontinuities in host strata that can be tracked from MVS eruptive centres to depths of at least 4 km (plumbing-type 5). This plumbing style does not show branching or lateral migration, and could potentially represent simpler source-to-surface magmatic pathways from deeper magma chambers.

An analogy for dikes in the MVS is provided by a network of dikes and sills intruding poorly indurated Eocene marine strata from outcrops in the inland Canterbury Basin (Figure 8). These intrusions show distinctive outcrop patterns dependent on their emplacement depths. Deeper level intrusions mainly comprise sub-vertical dikes in sharp contact relationship with their host sandstones (Figure 8). Shallower intrusions have magma-finger terminations associated with thin sill apophysis and peperitic borders. Tens of meters up-sequence (and above the intrusions), calcite veins occur cross-cutting sedimentary strata in the absence of hypabyssal rocks, suggesting migration of fluids above these intrusions.

Disrupted blocks

Disrupted blocks are recognized in 2D seismic lines by parallel reflectors with abrupt lateral discontinuities (Figure 6; Figure 9A and B). These seismic facies are interpreted to represent host

sedimentary strata intensively deformed and cross-cut by intrusive bodies. Disrupted blocks typically occur below eruptive centres and in association with plumbing-types 3, 4 and 5, or above and lateral to intrusive bodies of plumbing-types 1 and 2 (Figure 4; Figure 5; Figure 6). These discontinuous "blocks" are likely formed due to fracturing, faulting and forced-folding of host strata, to accommodate deformation caused by the emplacement of intrusive bodies (e.g. Hansen and Cartwright, 2006; Jackson et al., 2012; Bischoff et al., 2017). Another possible mechanism that could potentially form disruptive blocks are the emplacement of multiple intrusions closely spaced apart, such as the field example shown in Figure 9C and D. Rupture and faulting of host sedimentary strata can be an important process for creating pathways for magma and/or fluid migration within the basin strata (e.g. Sversen et al., 2017; Montanari et al., 2017).

Jacked-up domes and the MVS pre-eruptive dome

Jacked-up domes are formed by uplift of pre-eruptive sedimentary strata above large intrusions (Figure 4; Figure 10; Figure 5; Figure 6; Figure 9). In the study area, these dome structures are commonly associated with saucer-shaped sills (plumbing-type 1), and vary in diameter from 1 to 5 km. Complex fracture/fault networks with both normal and reverse faults are often observed along the borders of domed structures (e.g. Hansen and Cartwright, 2006; Montanari et al., 2017), which could provide conduits for magma and fluids as they ascend up-sequence (plumbing-type 3). In the MVS, the isochron map corresponding to the top of the early Miocene shows a semi-elliptical area of 1,137 km^2 that contains several 4-way dipping structures with maximum vertical relief of ca 100 m, located above large saucer-shaped intrusions and/or dikes-and-sills swarms (Figure 10). A possible explanation for this semi-regional uplift (pre-eruptive dome) is that the large size of swarms of intrusions emplaced within the sedimentary basin may produces inflation and ground dilatation above the MVS plumbing system, as example of the dome beneath Kora volcano shown in Bischoff et al. (2017), Infante-Paez and Marfurt (2017)

and Morley (2018). Another possible explanation is that the pre-eruptive dome could be influenced by thermal uplift, representing a small scale process of what is interpreted as the mechanisms that have formed the Ethiopian and Kenya domes (e.g. Macdonald, 2003; Chorowicz, 2005; Ring, 2014).

Stocks and laccoliths

Seismic anomalies associated with plumbing-types 2 and 3 show high amplitude reflectors with irregular and concave downward shapes (Figure 6). These anomalies cross-cut enclosing strata and produce a domed configuration in enclosing strata immediately above the anomalies. These bodies have been interpreted to represent small (< 200 m) stocks that intruded pre-magmatic sedimentary sequences. Laccoliths possible occur in the plumbing-types 2 and 3, however separating them from stocks is not possible in the seismic data from the MVS due to lack of resolution of 2D seismic data.

In summary, the plumbing system of the MVS is characterised by a complex network of sills and dikes that deform pre-magmatic sedimentary strata. Many of these intrusions (i.e. large saucer-shaped sills of plumbing-type 1) served as stationary shallow magmatic chambers that fed eruptions at the middle Miocene seabed. In other cases, a deeper source-to-surface (plumbing-type 5) is likely to have fed some submarine volcanoes. Seismic images of the MVS plumbing system suggest that a greater volume of magma has been emplaced within the basin sedimentary strata of the basins, in contrast with a much smaller volume that reached the paleo seabed (e.g. Figure 5).

Syn-eruptive architectural elements: eruptive, eruption-related and contemporaneous non-volcanogenic sedimentary deposits
Syn-eruptive architectural elements are cogenetic sets of eruptive, eruption-related and time-equivalent non-volcanogenic sedimentary rock units formed during the active constructional

stage of the MVS. During the constructional stage, the architecture of the volcanoes in the MVS was mainly controlled by interactions between internally (i.e. magma composition, pressure and magma ascension rate) and externally (i.e. interaction with water, soft or hard country rock and presence of pre-existent structures) driven mechanisms of fragmentation, dispersion and volcanic edifice growth. These processes controlling volcanic morphology and architecture are commonly observed in active volcanoes and is typicaly interpreted from ancient outcropping ancient volcanic systems (e.g. White, 2000; Kereszturi and Németh, 2013).

Two main volcano-morphologies were observed in the MVS seismic data: (i) crater-type and (ii) cone-type volcanoes. Each of these volcano-types contains distinctive combinations of cogenetic sets of syn-eruptive architectural elements at different scales, although some elements can occur in both volcano-types (e.g. tephra fallout carpets). We observed that the seismic morphological aspects of these buried volcanoes show similarities to subaerial and submarine monogenetic volcanoes well documented in the literature elsewhere (e.g. Lorenz, 1985; Cas et al., 1989; White, 1996; Lorenz and Kurszlaukis, 2007; White, 2000; Corcoran and Moore, 2009; White and Ross, 2011; Kaulfuss et al., 2012; Kereszturi and Németh, 2013; Jones et al., 2017; Reynolds et al., 2017; Figure 11; Figure 13; Figure 14). These similarities assist our interpretations and provide information for the construction of a comprehensive time-space framework showing the distribution of different sets of architectural elements for each volcano-type.

Crater-type volcanoes: deep-water equivalent of maar-diatreme volcanoes

Crater-type volcanoes of the MVS are characterised in seismic reflection imagery by funnel and basin-like excavations into pre-magmatic sedimentary strata. Reconstructed MVS diatremes (Bischoff, 2019) vary in diameter from 901 to 1682 m, and show 91 to 230 m in depth excavated into the PrErS. These pit craters were formed into relatively soft ground, locally corresponding to the bathyal Tokama siltstone in the upper part, and to the micritic Amuri limestone and Ashley mudstone in the root zone (Figure 11). Basin-like excavations are rare in the MVS and difficult

to characterise due to seismic resolution limitations, thus, further descriptions consider only morphological aspects of funnel-like volcanoes. The architecture of MVS crater-type dominate volcanoes can be divided into eight distinctive fundamental architectural elements: (1) root zone, (2) lower and (3) upper diatreme, (4) tephra ring, (5) ring plain, (6) intra-crater cones, (7) overspill wedge and (8) tephra fallout carpet (Figure 11; Figure 13; Figure 14). The main aspects of the large-scale architecture of crater-type dominate volcanoes are presented in Table 3.

Based on the presence of disrupted reflectors showing minor depressions located at the base of the diatreme structures (Figure 11; Figure 13), we interpret that the bottom part of the diatremes in the MVS may contain a *root zone* (Figure 9; Figure 10; Figure 11). Studies elsewhere suggest that this zone is the locus of thermohydraulic explosions (e.g. Lorenz, 1985; Lorenz and Kurszlaukis, 2007; White and Ross, 2011; Kereszturi and Németh, 2013), and likely contains syn-intrusive architectural elements such as contact breccias, disrupted pre-magmatic blocks, and late intrusive plugs. However, we do not recognize indicative seismic facies that could support the occurrence of these elements, perhaps because they are seismically unresolved. In some cases, the possible location of the root zone is coherent with seismic reflectors that correspond to the Amuri and Omihi limestones, and maybe to Charteris Bay Sandstone in its deepest part (Figure 13). The MVS volcanoclastic rocks sampled in Resolution-1 from 1140 to 1150 m contain numerous lithics of limestone and white very-fine sandstone (Figure 12), which may provide evidence that the country rocks of the root zone have experienced intense fragmentation, and were incorporated into the material ejected by high energy explosive eruptions. In diatremes of the MVS, the depression at the centre of the funnel-like structure may indicate post-eruptive subsidence (Figure 13).

The *lower diatreme* show an unbedded and chaotic structure below the PrErS (Figure 11; Figure 13), which suggest that pre-magmatic sedimentary strata were deformed in this location. These deformed strata could indicate processes such as fracturing of the host rock due to shockwaves,

16

crater wall brecciation and blocks collapsing during large explosive activity (e.g. Kereszturi and Németh, 2013). Another possible process responsible for the unbedded-chaotic seismic aspect of the lower diatreme zone is the formation of intra-diatreme faults, developed during post-eruptive subsidence (e.g. Lorenz, 1985; White and Ross, 2011; Kereszturi and Németh, 2013; Jones et al., 2017). The presence of feeder intrusions (plumbing-type 4 and 5) are likely to occur in the lower diatreme, supported by seismic images showing sub-vertical to sub-horizontal moderate amplitude reflectors in association with disrupted pre-magmatic blocks (Figure 11; Figure 13). Intrusive bodies located in the lower part of maar-diatreme volcanoes are commonly observed from outcrops elsewhere (e.g. Lorenz, 1985; White and Ross, 2011; Kereszturi and Németh, 2013).

The *upper diatreme* (Figure 11; Figure 13) is located immediately above the lower diatreme. This architectural element, in contrast from what is observed in the lower diatreme, is characterized by bedded structure, evidence of the presence of rock bodies deposited sub-horizontally to each other. The seismic aspect of the upper diatreme suggest that this zone is composed of alternating layers, perhaps layers of tephra material sourced from late stage eruptions, together with possible slumps, slides and debris deposits that infill the top part of the diatreme (Figure 11). Similar stratigraphic relationship is observed in analogue diatremes elsewhere (e.g. Lorenz, 1985; White and Ross, 2011; Kereszturi and Németh, 2013). Together, the lower and upper diatremes possible indicate the location of an eruptive vent zone.

Laterally and symmetrical to the both sides of the diatreme, we observed a distinctive parallel and continuous high amplitude reflector located immediately above PrErS (Figure 11; Figure 13), which we interpreted to correspond to the *tephra ring* and *ring plain* a of a maar-diatreme volcano. Morphological and morphometric reconstruction of the MVS volcanoes (Bischoff, 2019) suggest that these reflectors are inclined at ca 20° near to the vent zone. These reflectors become progressively sub-horizontal and parallel with basin strata reflectors with increasing

distance from the vent (Figure 11; Figure 13). Their high amplitude continuous seismic aspect fade-out to become semi-continuous, moderate-to-low amplitude (this last, is the characteristic seismic facies of Tokama siltstone). This "fading-out" phenomenon of seismic reflectors with increasing distance from an eruptive centre have been interpreted to mark the transition of volcanic to sedimentary rocks (Herzer, 1995; Reynolds et al, 2017). It is possible to map the lateral extension of the high amplitude reflectors for ca 5 km from both sides of the diatreme structure, which suggests that these reflectors likely represent material dispersed from the vent zone, possibly formed by high energy explosive eruptions. We interpret the steeply inclined reflectors located proximal to the diatreme zone to correspond to the tephra ring of a maar volcano (Figure 11; Figure 13), formed by accumulation of tephra ejected as ballistic material during pyroclastic eruptions. At its thickest part, this tephra ring may be as thick as 20 m (Bischoff, 2019). The lateral continuity of the tephra ring is represented by sub-horizontal high-amplitude reflectors, which we interpret to correspond to material deposited in the ring plain of a maar volcano (Figure 11; Figure 13). In plain view, the ring plain of some MVS volcanoes shows a semi-circular geometry with ca 10 km of lateral extent (Bischoff, 2019), which reinforce the hypothesis of high energy explosive eruptions forming this architectural element.

In the seismic data of the study area, the bedded diatreme is typically overlain by a dome- and cone-like structure limited by the internal flanks of the tephra ring (Figure 11; Figure 13). This zone is interpreted to represent material that accumulate inside the negative crater morphology of a maar-diatreme volcano. Based on the convex upwards seismic facies of this zone, and in association with examples described in the literature (e.g. Lorenz, 1985; Kereszturi and Németh, 2013), we interpret these seismic facies to correspond to *intra-crater cones* formed by accumulation of tephra, and maybe minor hyaloclastite and pillow-lava material deposited in the crater zone during late stage eruptions.

Lateral to the intra-crater cone and overlaying the tephra and ring plains, we observe a characteristic seismic facies composed of discontinuous moderate-amplitude reflectors, here referred to as the *overspill wedge*. This wedge have a maximum lateral extension of ca 7 km, and typical reconstructed vertical heights of ca 30 m (Bischoff, 2019). Such as observed in the tephra ring and ring plain, reflectors of the overspill wedge merge and fade-out with increasing distance from the eruptive centre (Figure 13). We interpret this architectural element to represent fragmented material that overspills the tephra ring by ballistics and other dispersion mechanisms related to submarine eruptive plumes (e.g. eruption-fed density currents; White, 2000). The overspill wedge may also contain minor pillow-lavas and hyaloclastite deposits (e.g. Kereszturi and Németh, 2013), interbedded to deposits from explosive submarine eruptions. However, we did not identify seismic facies that could confirm the presence of lava deposits in the overspill wedge, perhaps due to lack of seismic resolution.

The presence of thin tuffaceous layers interbedded with the Tokama siltstone (Bischoff, 2019) suggests that tephra material could be transported and deposited for long distances from the MVS vents. Studies of the deposits of submarine eruptions (e.g. Fiske et al., 1998; Bonadonna et al., 2002; White, 2000; Deardoff et al., 2011; Cas and Giordano, 2014), show that submarine eruptions can eject significant amount of tephra into the water column. This material can be transported in suspension and be deposited distal to the eruptive centre as thin and tabular layers of tephra. Based on these evidences, we interpret the presence of a *tephra fallout carpet* occurring in distal parts of the maar-diatreme volcanoes (Figure 11; Figure 13), however, this architectural elements is seismically unresolved.

Cone-type volcanoes: deep-water equivalent of tuff cones.

In contrast to their counterpart crater-type volcanoes, MVS cone-type volcanoes are characterised in seismic imagery by a sequence of reflectors that pile-up close to the vent zone, forming convex upwards curvature of the PoErS above PrErS, and minor excavation into the pre-

eruptive strata (Figure 15; Figure 16; Figure 17; Figure 18). This volcano-type typically occurs as isolated cones, ranging in average size from 1 to 3 km in diameter, and 100 to 300 m in height (Bischoff, 2019). Seismic data show that the sub-vent zone of this volcano-type (Figure 15) contains shallow high-amplitude reflectors that may represent intrusions related to plumbing-type 4 (Figure 6). Most MVS cone-type volcanoes appear to be fed by large sill intrusions related to plumbing-type 1 and 3. The exception is the overlapped volcanic cluster (Figure 6) that appears to be fed by plumbing-type 5, and does not show evidence to be fed by a shallow (< 4 km) magmatic chamber.

The syn-eruptive architecture of the cone-type volcanoes of the MVS can be divided into five fundamental elements, based on distinctive seismic facies, and on surfaces that bound characteristic morphologies. These architectural elements are: (1) basal cone, (2) central crater, (3) tephra flank, (4) cone apron, (5) tephra fallout carpet. As is the case for crater-type dominate volcanoes, each one of these five large-scale parts may contain individual or sets of cogenetic architectural elements (Figure 15; Figure 16; Figure 17; Figure 18). The main characteristics of the syn-eruptive architectural elements of this volcano-type are shown in Table 4.

The *basal cone* is characterised by sub-horizontal and parallel reflectors of high to moderate amplitude that are located near the interpreted vent zone. This architectural element typically shows stacked high-amplitude reflectors, suggesting that the basal cone contains layers of relatively dense material, perhaps indicating the presence of deposits such as submarine lavas and hyaloclastites formed during the initial eruptive stages of the cone construction (Figure 6, type 5). However, it is also commonly observed that the geometries and seismic character of the basal cone is seismically similar to the tephra flank, comprising low amplitude reflectors which may indicate deposition of layered tephra at this zone (see further explanation for the interpretation of the tephra flank in this sub-chapter). Based on the presence of high amplitude reflectors cross-cutting sub-horizontal reflectors (Figure 6; Figure 15), it is likely that the basal

cone also contains minor shallow intrusions (plumbing type-4), which are commonly observed in monogenetic volcanoes (e.g. Kereszturi and Németh, 2013).

The *central crater or vent zone* is characterised by disrupted, chaotic and layered reflectors dipping inward toward the centre of the cone structure (Figure 12; Figure 13; Figure 15), evidence that deposits has infilled a negative shallow depression at this location. This architectural element is typically located above seismic facies (i.e. disrupted pre-magmatic reflectors, high amplitude reflectors cross-cutting enclosing strata) that indicate the presence of magmatic conduits and intrusive bodies (e.g. McLean et al., 2017; Bischoff et al., 2017; Infante-Paez and Marfurt, 2017; Morley, 2018). The structure of the central crater shows minor excavation into the PrErS horizon, which suggest that the eruptions in cone-type volcanoes were much less damaging to the to host rocks beneath the vent, in contrast with the deep diatremes observed in the crater-type volcanoes (e.g. White and Valentine, 2016). We interpret this architectural element to be formed by explosive eruptions and associated jets of tephra, which create space for subsequence deposition of chaotic and amalgamated layers of tephra inward-dipping into the central crater. Observations in ancient outcropping submarine monogenetic volcanoes of Waiareka-Deborah offshore Oamaru, South Island of New Zealand (e.g. Cas et al., 1989; Corcoran and Moore, 2009; Moorhouse; 2015) show that the crater zone of those volcanoes typically contain massive, chaotic, to amalgamated deposits of lapilli-tuff to tuff-breccia, formed by tephra jets and ballistics during explosive eruptions, and deposits of tephra dipping inwards in the crater zone (Figure 17A, B and C). Deposits of the central crater of the Waiareka-Deborah have ben reworded by gravitational processes (Corcoran and Moore, 2009).

The *tephra flank* of the volcanoes in the MVS is characterised by inclined, low-to-moderate amplitude reflectors dipping outward from the centre of the cone-like structure (Figure 15; Figure 16). We interpret the flanks of MVS cone-type volcanoes to predominately contain fragmented material that originated from submarine pyroclastic eruptions, rather than

subaqueous lava deposits. This interpretation is supported by: i) a clear lateral relationship of the tephra flank with a crater (vent) zone that suggests explosive activity, ii) seismic facies showing low-to-moderate amplitude[1], semi-continuous, parallel and inclined reflectors, symmetrically dipping away from the vent zone[2], iii) rock-types collected in the Resolution-1 well that evidence explosivity[3] (e.g. peloidal fragments enveloped by palagonite films, armoured lapilli?, broken crystals, relics of bubble walls, and high vesiculated rocks; Figure 12). However, some minor lavas and hyaloclastite deposits are commonly observed in explosive monogenetic volcanoes elsewhere (e.g. Kereszturi and Németh, 2013), thus, these deposits (and maybe type-4 intrusions) are expected to occur in the tephra flank, evidenced by localized and isolated high-amplitude reflectors (Bischoff, 2019). Observations from outcrops in the Waiareka-Deborah volcanoes suggest that their flanks were constructed by multiple explosive eruptions with minor interruptions, in which dispersion of material was induced by mechanisms such as tephra jets, ballistics, grain flow, debris remobilization, and eruption-fed density currents (e.g. Cas et al., 1989; Corcoran and Moore, 2009; Kaulfuss et al., 2012; Moorhouse; 2015). Deposits on the flanks of those volcanoes are typically tabular and composed of thin-bedded layers of tephra dipping away from the vent zone (Figure 17A, C and D). Eruption-fed density currents usually form well-sorted and thinly-bedded pyroclastic deposits that show similarities to the Td and Te turbidite facies of the Bouma sequence (e.g. Cas et al., 1989; White, 1996; Corcoran and Moore, 2009; White, 2000; Di Capua and Groppelli, 2016). These bedded rock facies are possible to occur in the tephra flanks of the MVS volcanoes.

---

[1] Typically, lava deposits show high-amplitude continuous reflectors. Volcanoclastic material usually show moderate amplitude (e.g. Planke et al., 1999; Reynolds et al., 2017).

[2] This stratal relationships are commonly observed for deposits formed by explosive eruptions in both subaerial and submarine environments (Cas et al., 1989; White, 1996; White, 2000; Kereszturi and Németh, 2013),

[3] These textures alone are not diagnose for explosivity, but could also represent submarine auto-brecciation (e.g. White and Valentine, 2016; Cas and Simmons, 2018). Because of this, our interpretations are made in association with the seismic aspects (e.g. morphology, seismic facies) of the volcano-types).

The *cone apron* architectural element is characterised by sub-horizontal and parallel reflectors that pinch and amalgamate with basin reflectors with progressive distance from the cone structure (Figure 15; Figure 16). The Resolution-1 well likely penetrates the distal cone apron of a MVS cone-type volcano at depths of 1103.5 to 1114 m, recovering thin tephra layers interbedded with siltstones (Bischoff, 2019). Based on this evidence, we interpreted the cone apron to contain fine-grained layers of tephra transported by subaqueous eruption plumes, likely interbedded with reworked material from cone collapses and degradation, a phenomena commonly observed in volcanoes elsewhere (e.g. White, 1996; Kereszturi and Németh, 2013; Pope et al., 2018). The cone apron likely contains minor subaqueous lavas that overspill from the crater rim (and possible peperitic material associated with invasive lavas and/or shallow type-4 intrusions; e.g. Planke et al., 2017), as indicated by the localized high-amplitude reflectors that occur in association with this element (Bischoff, 2019). The interpretation of 3D seismic dataset containing of lava-flows associated with submarine monogenetic volcanism along the southern Australian margin shows that submarine lava flows could extend for more than 34 km in length from the eruptive centre (Reynolds et al., 2017).

The *tephra fallout carpet* of cone-type volcanos (like their counterpart crater-type volcanoes) is typically seismically unresolved and based on studies elsewhere (e.g. Fiske et al., 1998; Bonadonna et al., 2002; White, 2000; Deardoff et al., 2011; Cas and Giordano, 2014). Volcanoclastic rocks interbedded with the Tokama Siltstone recovered in the Resolution-1 well from 1114 to 1200 m depth may represent this element in cone-type volcanos of the MVS (Bischoff, 2019). Submarine eruption plumes (and also subaerial pyroclastic density currents entering the water) can introduce pyroclasts and rock fragments into the water column, while residual buoyant material can remain suspended and be transported by oceanic currents (e.g. Fiske et al., 1998; Bonadonna et al., 2002; White, 2000; Deardoff et al., 2011; Cas and Giordano, 2014; Di Capua and Groppelli, 2016). Rafts of highly vesiculated pumice can travel long

distances carried out by currents (Rotella et al., 2013; Cas and Giordano, 2014; Cas and Simmons, 2018). When saturated in water, these fragments sink and can form deposits with size varying from ash to blocks (e.g. Fiske et al., 1998).

Aiming to better understand the distribution of architectural elements in the cone-type volcanoes of the MVS, we contrast they seismic facies architecture with examples of volcanoes buried in Eocene strata in the Canterbury Basin, ca 40 km offshore of Oamaru (e.g. Barrier et al., 2017; Figure 15). These buried Eocene volcanoes are likely part to the Waiareka-Deborah Volcanic Field, and show similarities with the buried volcanoes of the MVS. As in MVS, the sub-vent zone of these volcanoes contains disrupted blocks and high amplitude reflectors that cross-cut pre-eruptive strata, which likely represent intrusive bodies and magmatic conduits. Above the conduit zone, the presence of chaotic seismic facies indicates the location of the central crater. Laterally to the central crater, symmetrical inclined reflectors outward-dipping represent the tephra flank. Distal to the tephra flank, these reflectors become sub-horizontal and parallel to basin strata, producing the seismic-equivalent expression of the cone apron. At the top of the edifice, reflectors have a domed configuration, which is commonly interpreted as the product of differential compaction during burial of volcanoes (e.g. Planke et al., 2000; Bischoff et al., 2017). The above described similarities could indicate that cone-type volcanoes of the MVS experience similar fragmentation and dispersion processes as those from the Waiareka-Deborah volcanic field, those interpreted to be formed by phreatomagmatic eruptions (e.g. Cas et al., 1989; Corcoran and Moore, 2009; White and Ross, 2011; Kaulfuss et al., 2012).

Eruption-related sedimentary architectural elements
Sedimentological and volcanological processes observed on modern volcanoes (e.g. White, 1991; Cas and Wright, 1992; Chadweck et al., 2012; Kereszturi and Németh, 2013; Pope et al., 2018) suggest that the syn-eruptive interval of the MVS may comprise sedimentary deposits triggered by simultaneous eruptions, together with primary volcanic eruptive deposits. Processes

related to the eruptions such as earthquake shockwave, explosions, and magmatic inflation are potential triggers for debris flows, submarine landslides and cone-sector collapses (e.g. submarine landslides triggered by the 2009 eruption at NW Rota-1 volcano, Mariana arc; Chadweck et al., 2012). Tephra material can be reworked during or immediately after eruptions by mechanism such as submarine currents, waves and tsunamis (e.g. Kereszturi and Németh, 2013; Shumaker et al., 2018). Based on the available 2D seismic data and limited number of wells, distinguishing eruptive volcanic deposits from eruption-related sedimentary deposits, or from resedimented epiclastic deposits is not always possible. We tentatively infer five settings (Figure 4; Figure 11; Figure 15; Figure 19) in which distinctive sets of eruption-related sedimentary architectural elements can form, based on seismic facies (e.g. chaotic reflectors, sediment waves) that could indicate reworking of parts of the volcanic edifices during eruptions. These settings are: (1 and 2) the crater zone of both volcano types; (3) the flanks of cone-type volcanoes; (4) the tephra ring of crater-type volcanoes; (5) the cone apron of cone-type volcanoes.

Seismic images and analogues elsewhere suggest that the crater zone of MVS volcanoes may contain sedimentary deposits controlled by gravitational flows and other types of mass transport deposits that infill the space created by explosions and by ground collapses during (and immediately after) eruptions. Common sedimentary facies in the crater zone may include course-grained, massive, chaotic and amalgamated deposits formed by tephra reworking and slip into the crater (Figure 17 B and C), and by slide and slump blocks from the crater walls (e.g. White and Ross, 2011; Kereszturi and Németh, 2013; White and Valentine, 2016). On the flanks of cone-type and along the tephra ring of crater-type volcanoes, material reworking by currents and mass-wasting are important syn (and post) eruptive process (e.g. Cas et al., 1989; Fiske et al., 1998; Corcoran and Moore, 2008; Pope et al., 2018). On the cone apron of a cone-type volcano of the MVS (Figure 19), seismic images show a characteristic facies that resembles sediment

waves occurring between the PrErS and PoErS horizons, which may represent syn-eruptive submarine landslides such as those reported by Pope et al. (2018).

Inter-eruptive architectural elements

Monogenetic volcanic fields are typically characterised by a cluster of dispersed and isolated volcanoes formed by one eruptive cycle with minor interruptions (e.g. Németh, 2010; Kereszturi and Németh, 2013; Silva and Lindsay, 2015; Németh and Kereszturi, 2015). Individual volcanoes are typically diachronous with one another, and have an active life of years to centuries (e.g. Silva and Lindsay, 2015), and hundreds of thousands to a few million years for the complete volcanic field (e.g. Connor and Hill, 1995; Hintz, 2008; Condit, 2010; Kiyosugi et al., 2010 apud Kiyosugi, 2012).

In our volcano-stratigraphic model (Figure 2; Figure 4), inter-eruptive architectural elements can be formed in association with volcanoes that have finished their eruptive cycle, but may start to degrade and interact with basin sedimentation while volcanism still active in other parts of the MVS. In contrast to polygenetic volcanoes, for where syn-and inter-eruptive deposits commonly are interbedded close to a relatively stationary eruptive centre, in monogenetic fields, these inter-eruptive sedimentary deposits can form in all extension of the volcanic field, typically interbedded with primary volcanic deposits erupted from diverse vents. In MVS, inter-eruptive architectural elements are represented by sedimentary rocks of the Tokama siltstone interbedded with volcanoclastic rocks that likely were erupted from different vents (e.g. Figure 19). In addition, inter-eruptive deposits related to mass transport and erosion of inactive volcanoes are likely to occur in MVS, however, we cannot separate these rock units from syn-eruptive sedimentary deposits, due to limitations in the seismic resolution of our dataset.

Post-Magmatic Sequence

Sedimentary processes such as erosion and burial of the volcanic edifice are dominant during the post-magmatic sequence (Figure 2; Figure 4). After the magmatic activity in the MVS had ceased at ca 11.5 Ma (Bischoff, 2019), the submarine volcanic morphology had a strong impact on the sedimentation patterns of the study area. We divide the post-magmatic sequence into degradational and burial stages. Each stage is marked by different processes of erosion and burial of the volcanic edifices, which control the formation and distribution of MVS post-magmatic architectural elements. Post-eruptive degradation has changed the original volcanic morphology, which was controlled by the height, and by the position of the volcanic edifices in relation to a late Miocene (lM) base-level fall (Bischoff, 2019). After volcanism ceased, volcanoes located in a bathyal setting were rapidly buried and preserved, while volcanoes located in a neritic setting and with edifice heights > 200 m were possibly emergent at the paleo sea-surface and have their tops flattened (Bischoff, 2019).

Degradational stage: rate of erosion > rate of burial

The degradational stage is marked by high rates of erosion of the volcanic edifices. In the MVS, we place the PoDgS coincident with the late Miocene (lM) unconformity (Figure 4), because this erosive surface represents the last significant event that degrade the volcanic edifices (Bischoff, 2019). Based on seismic reflection analysis, we identify architectural elements of this stage such as canyons, gullies, localized epiclastic deposits and contemporaneous non-volcanogenic sedimentary deposits impacted by the presence of the volcanoes (Figure 13; Figure 16; Figure 19). Canyons and gullies are usually associated to the PoDgS, varying in size from < 100 m to 1100 m wide and present internal channelized deposits (Figure 19; Figure 20) up to ca 175 m thick, considering a seismic wave velocity of 2500 m/s for this sedimentary strata (Bischoff, 2019). Channels are narrow towards shallow waters and wider and more deeply incised at the slope/abyssal interface, sometimes occurring stacked at the base of the tephra flank and cone

apron of cone-type volcanoes (Figure 19; Figure 20). Canyon erosion can removes material from the volcano flanks, which may cause instability and collapse of parts of the cone, forming localized small size debris deposits (Figure 4). However, if these debris deposits occur in the MVS they are seismically unresolved with the available dataset.

Volcanoes with flattened tops concordant with the PoDgS typically show reflectors downlapping from the edifice onto the basin floor, which suggests that these volcanoes provide a local source of epiclastic sediments (Figure 4; Figure 20). Seismic attribute analysis shows that these deposits likely contain material eroded from the volcanoes, due to their similarity in seismic impedance aspect in diverse seismic attributes (Figure 20). This degradational seismic facies only occurs in association with reconstructed volcanoes > 200 located proximal to the 11 Ma shelf-break position (Bischoff, 2019). We interpret this facies to represent a plume of epiclastic sediments eroded from volcanoes that were emergent and/or eroded in a shallow submarine environment by the action of waves and shallow currents. The epiclastic plume is deposited parallel with the direction of the prograding clinoforms, with maximum seismically detected horizontal and vertical dimensions of up to 3 km and 70 m respectively, and probably represent sediments deposited next to extinct volcanic islands (Figure 20). Similar seismic facies are evident in the Vulcan-3D, located in the offshore Taranaki Basin (Bischoff, unpublished data).

Between the cone-type volcanoes, a characteristic seismic facies is observed, comprising of horizontal and parallel continuous reflectors, here referred to as inter-cone plains (Figure 19; Figure 20). The seismic facies of the inter-cone plains are similar (moderate amplitude, semi-continuous and parallel reflectors) to those where the well Resolution-1 recovered fine-grained sedimentary rocks of the Tokama siltstone. This seismic character suggests that the inter-cone plains were mostly confined between volcanic edifices and formed by non-volcanogenic sedimentary strata deposited by processes of decantation in a low energy environment. However,

minor epiclastic deposits may occur next to the flanks of the volcanoes, interbbeding with sediments of the inter-cone plains.

Burial stage: rate of erosion > rate of burial

In seismic imagery, the burial stage of MVSis characterised by facies showing evidence that the volcanic edifies impacted local sedimentation for a long time after these structures were buried. This stage in the MVS is marked by high rates of burial and little or non-degradation of the volcanic edifices that remained unburied after the lM unconformity (i.e. PoDgS). Seismic reflectors above eleven cone-type volcanoes display a domal structure, here referred to as burial dome, suggesting the presence of a persistent bathymetric high after these volcanoes were buried. The processes that resulted in the production of the burial dome likely include differential compaction between volcanic and enclosing sedimentary strata (e.g. Planke et al, 2005; Bischoff et al., 2017; Holford et al., 2017). Because the impact of buried volcanoes in the basin architecture varies from one volcano to another, we place the PoBuS according to observations from pc14. Canyons scars located on the edges of the burial dome above pc14 (Figure 19) evidence that this edifice impacted basin sedimentation until the Opoitian (5.3 to 3.7 Ma), at least ca 6 Ma after volcanism in the MVS has ceased, and ca 1 Ma after pc14 was completely buried at around 5 Ma. Seismic images of this peripheral canyons (i.e. around the margins of the burial domes) are likely to be associated with the deposition of submarine fans up to 2 km wide (Figure 19). Fans such as these are well imaged from 3D seismic data over the buried Kora Volcano, offshore of Taranaki Basin, which were referred to as seamount-edge fans by Bischoff et al. (2017). The processes that control the deposition of these fans remains poorly investigated, but are likely either to involve erosion around the burial dome due to local formation of a hard seafloor substrate associated with the dome structure, or could be related to carbonate deposits at the top of the domes.

Discussion

Origin of the crater-type volcanoes in the MVS

Crater-type volcanoes of the MVS contain syn-eruptive architectural elements that show deep craters excavated into the PrErS horizon, and associated deposits that suggests substantial material dispersion laterally to these craters. Deep excavations into the PrErS requires significant energy and intense material fragmentation (e.g. Zimanowski et al., 1997). White and Valentine (2016) suggest that the funnel-like structure of maar-diatreme volcanoes, in association with dispersed lateral tephra deposits, may be one of the most direct evidence for dominant phreatomagmatic activity. In subaerial and shallow subaqueous environments, it is widely accepted that basaltic maar-diatremes result from phreatomagmatic eruptions (e.g. White and Valentine, 2016). Zimanowski and Büttner (2003) argue that subaqueous volcanic thermohydraulic explosions become increasingly improbable at water depths > 100 m, and practically impossible at water depths > 1000 m. However, Agirrezabala et al., (2017) describe two Albian deep-water diatremes and associated volcanoclastic deposits at a well-exposed outcrop of the northern margin of the Basque-Cantabrian Basin (north Iberia). This authors interpreted the diatremes as formed mainly by phreatomagmatic mechanisms at water depths around 200 to 500 m. Clague et al. (2000) inferred that phreatomagmatic eruptions at the Loihi seamount offshore Hawaii occurred at a minimum depth of 1356 m, which is approximately equivalent to the depth of the root zone of the volcanoes studied here. In addition, examples of deep-water diatremes have been interpreted from seismic reflection data (Jamtveit et al., 2004; Svensen et al., 2004; Planke et al., 2005; Hansen, 2006) although their hydrothermal vs. magmatic origin still controversial.

Some rock-types recovered from Resolution-1 have textures that indicate intense material fragmentation (rocks composed of very-fine broken crystals and glassy shards with platy and cuspate shapes), and deposits that commonly contain limestone and sandstones lithics,

potentially sourced from the root zone of the MVS diatremes (Figure 12; Figure 13), which maybe represent of fallout material formed by submarine pyroclastic eruptions in the MVS (Bischoff, 2019). Cas and Simmons (2018) suggest that subaqueous effusive eruptions can produce fallout deposits of ash size autoclastic vitric material, similar to typical deposits of subaqueous pyroclastic eruptions. This autoclastic process could explain the large (ca 5 km) seismically detected limits of our ring plain and overspill wedge architectural elements, without necessarily requiring large explosive eruptions, but cannot explain the pit craters excavated into the PrErS horizon. We consider an autoclastic explanation for the crater-type volcanos of the MVS implausible, as their morphology suggests high-energy mechanisms of fragmentation and dispersion of material (e.g. Lorenz, 1985; White, 2000; Kereszturi and Németh, 2013; White and Valentine, 2016). In addition, the ring plain and the overspill wedge elements observed in the MVS indicate that material was deposited symmetrically on both sides to the diatreme structure (Figure 9; Figure 10), with distal representative rock-types of these architectural elements possibly recovered by the Resolution-1 well, containing textures that indicate intense material fragmentation (Figure 12). These observations together suggest that the crater-type volcanos in the MVS were likely formed by high-energy explosive eruptions, such as those triggered by phreatomagmatic processes. The geometry and spatial arrangement of the architectural elements in the crater-type volcanoes suggests they are likely to represent the deep-water equivalent of maar-diatremes (funnel-like structure) and maybe tuff rings (basin-like structure), formed by high-energy explosive eruptions in a subaqueous environment around 1000 m deep.

Origin of the cone-type volcanoes in the MVS

MVS cone-type volcanoes contain syn-eruptive architectural elements that shows reflectors pilling-up above the PrErS horizon, next to an interpreted vent zone with little or no excavations into the PrErS horizon. White and Valentine (2016) state that the vent structure and associated ejecta deposits may be the best evidence that characterises past eruptive processes in

monogenetic volcanoes. These authors infer that volcanoes dominated by purely magmatic volatile-driven processes have discrete explosions when compared with those dominated by phreatomagmatic activity, a process that is much less damaging to host rocks beneath the vent. In mafic systems that form cone-type volcanoes (e.g. scoria cones), explosions are typically manifested as Strombolian and Vulcanian-types (e.g. Kereszturi and Németh, 2013; White and Valentine, 2016). However, cone-type volcanoes (e.g. tuff cones) can also form by phreatomagmatic processes (e.g. Cas et al., 1989; White, 1996; White, 2000). In fact, the final morphology of a monogenetic volcano does not necessarily represent a single eruptive-style, but more commonly these morphologies result from simple or complex edifice growing mechanisms (Kereszturi and Németh, 2013), which makes the recognition of past eruptive events difficult based exclusively on morphological parameters. However, the vent structure of cone-type volcanoes of the MVS shows minor excavation into the PrErS horizon, which suggests that the effects of eruptions on the host rocks are minimal, when compared to those of crater-type volcanoes. Further, the predominance of inclined, low-to-moderate amplitude reflectors dipping symmetrically outward from the centre of the cone-like structure suggests that the flanks of the cone-type volcanoes are mainly comprise of fragmented material, probably (radially?) ejected by pyroclastic eruptions rather than the deposits of effusive eruptions. The predominant low slope angles (< 16º in inclination; Bischoff, 2019) of the cone-type volcanoes in MVS, in association with the rock textures (e.g. possible armoured lapilli and ash aggregates) recovered in Resolution-1, and the widespread (up to 6 km) seismically detected extension of the tephra flank and cone apron together, suggests that this volcano-type is likely to represent a deep-water equivalent of a tuff-cone. However, we do not discard the possibility of the occurrence of spatter cones and pillow mounds in the MVS, which could be verified by acquiring additional high quality 3D seismic data and/or drilling holes into these volcanoes proximal to their vents.

Implications for Geoenergy Resources

In this section, we show how insights from the analysis of architectural elements of the MVS can be applied to the exploration of geoenergy resources such as hydrocarbons and geothermal energy. In both cases, subsurface fluid-dynamics are strongly influenced by the presence of architectural elements that can store, conduct or entrap fluids such as water, oil and gas (e.g. Schutter, 2003; Stimac et al., 2015). Here we present two models to illustrate possible combinations of architectural elements that favour the formation of petroleum accumulations and geothermal fields in association with volcanism. Understanding the geological conditions that form "fossil" magmatic systems in sedimentary basins is important for assessing the exploration risks, and to improve the likelihood of finding commercially viable energy resources in active intrusion-related hydrothermal systems. However, it is important to observe that these models are a simplified representation of a great number of variables with associated uncertainties. These models were built to provide guidelines for the potential of buried and active volcanoes to contain geoenergy resources within different stratigraphic parts of the volcanic system. Schematic representations presented in this section aim to illustrate how the architectural elements can possibly influence the subsurface dynamic fluid-flow of these systems. The conditions that determine if certain architectural elements have the ability to transmit or obstruct fluids are some of the key unknowns in any prospect evaluation. Given the large number of variables, the fluid-flow properties of volcanic systems will likely need to be considered on a case-by-case basis. To assess the risks and improve the likelihood of finding commercially important geoenergy resources in association with volcanic systems it is import to understand: (a) how these architectural elements are combined, (b) what are their petrophysical properties, and (c) how post-formational events can change their original characteristics.

Conceptual Petroleum Plays in Buried Monogenetic Volcanic Fields

To illustrate the great range of possible petroleum plays associated with buried monogenetic volcanic fields (Figure 21), we use the concept of a "petroleum system" from Magoon and Dow (1994). Here, this concept is applied to describe possible combinations of architectural elements and processes that are necessary to form hydrocarbon accumulations in different parts of a buried "MVS-type" system

Petroleum Elements of the Emplacement Stage

In the endogenous part of the system (emplacement stage), potential reservoirs can occur in both porous and non-porous host sedimentary rocks, with increasing permeability related to fracturing caused by the emplacement of magma (i.e. formation of the architectural element disrupted blocks), and in fractured intrusive bodies formed by thermal contraction during cooling (1 and 2 in Figure 21). An example of such fractured reservoir occurs in the Wichian Buri field in Thailand, where 30 Mbbl of oil and gas is contained in dolerite intrusions and associated sandstones (Remus et al., 1993; apud Schutter, 2003). Seals can be formed by fine-grained host sedimentary deposits and massive intrusions (e.g. Jurua field, Solimões Basin, Brazil; Barata and Caputo, 2007; 5 in Figure 21). Hydrothermal fluids can induce secondary porosity by mineral dissolution (e.g. Vieira de Luca et al., 2017; Mordensky et al., 2018; 3 in Figure 21), or can clog potential reservoirs by precipitation of cements (e.g. Schutter, 2003; 5 in Figure 21).

Intrusive bodies are likely to form many isolated or combined 4-way closures such as jacked-up domes above intrusions with sizes up to 30 km^2, mainly associated with the emplacement of saucer-shaped sills and dike-sill swarms (7 in Figure 21), such as those from plumbing-types 1 and 2 of the MVS. A combination of stratigraphic and structural traps can occur above sill intrusions or fractured rocks in contact with fine-grained sedimentary rocks, or in coarse-grained sedimentary rocks in contact with massive sills (8 in Figure 21). In the state of Montana (USA), many oil and gas fields with tens of millions of barrels were found in sandstones trapped by

intrusions (Lopez, 1995; apud Schutter, 2003). Fluids can migrate upwards through inclined porous host strata, fractured dikes, tectonic and magmatic induced fractures and faults (e.g. Holford et al., 2017; 13 and 14 in Figure 21). This fluid pathways can be associated with disrupted blocks, and be located above inclined sheets of saucer-shaped intrusions such those of plumbing-type 3 in the MVS (14 in Figure 21). Broken-bridge structures (i.e. elongate and discontinuous magma lobes located at the extremities of sill intrusions; e.g. Schofield et al., 2012) ca also act as a subvertical conduct subsurface fluids in the subsurface (11 in Figure 21). Lateral migration of hydrocarbons is possible in sub-horizontal coarse-grained host rocks, and/or below sills with fractured edges, and along the contact of permeable rocks with strata cemented by metasomatic activity or contact metamorphism (Figure 21).

Intrusions emplaced in organic-rich sedimentary rocks have the potential to elevate the geothermal gradient to ideal conditions and generate thermogenic gas (e.g. Aarnes et al., 2015). For example, heating by intrusions produced hydrocarbon accumulations with > 33 billion m^3 of gas in the Urucu province, Solimões Basin, Brazil (Barata and Caputo, 2007). Intrusions emplaced in organic-rich rocks can release high amounts of CO_2 and CH_4 (e.g. Delmelle et al., 2015; Svensen et al., 2017), and may release sulfidic acids (e.g. H_2S) if the host rocks, or the original magma was enriched in sulphur (e.g. Iacono-Marziano et al., 2013; Stimac et al., 2015; Robertson et al., 2015; Arnórsson et al., 2015). Magma emplaced in carbonate rocks can release CO_2 (e.g. Deegan et al., 2010; Blythe et al., 2015), which may be one possible explanation for the high content of this acid gas flooding some reservoirs in the prolific pre-salt sequence offshore of Brazil.

In summary, architectural elements of the constructional stage can impact the fluid dynamic of the emplacement stage with potential to host commercial hydrocarbon accumulations in fractured igneous rocks, and in porous and fractured host sedimentary rocks. Intrusions can

generate hydrocarbons or degrade their quality by adding gases such as CO_2 and H_2S into the system.

Petroleum Elements of the Constructional Stage

Potential reservoirs of the constructional stage comprise of eruptive and sedimentary deposits. Porous and fractured reservoirs can occur in lava deposits with vesiculated and brecciated margins and coherent cores with columnar joints formed due to cooling of lava (15 and 16 in Figure 21). In northwest Java, Indonesia, the Jatibarang field has produced 1.2 Gbbl of oil and 2.7 TCF of gas from andesitic rocks (Kartanegara et al., 1996; apud Schutter, 2003). Seismic images from the MVS suggest that lava deposits may occur at the basal cone and cone apron of cone-type volcanoes, and can extend as far as 3 km from the vent (16 in Figure 21). Pyroclastic rocks usually present high primary intergranular porosity due to fragmentation, which can be rapidly lost due to compaction during burial, or could also increase permeability by development of micro-fractures that connect pores (Heap and Kennedy, 2016; Heap et al., 2017). Observations in the Songliao Basin show that pyroclastic rocks have the potential to maintain high porosity and permeability at greater depths (up to 20% and 33 mD at depths of 1500 to 3500 m; Wang et al., 2018). Hyaloclastites, peperites, and pillow-lavas (Figure 21) can preserve primary and secondary porosity and have potential to form hydrocarbon reservoirs, as demonstrated from pillow-lava deposits of the Pão de Açúcar field. This field contain oil in primary volcanic vesiculated rocks, inter-pillow megapores, and pillow breccias (Vieira de Luca et al., 2017). Fine-grained contemporaneous sedimentary deposits, massive lavas, welded coarse-grained pyroclastic rocks, and ash deposits can form seals (e.g. Schutter, 2003; 19 in Figure 21). As well as in the emplacement stage, hydrothermal activity can induce secondary porosity, or cement reservoirs (e.g. Schutter, 2003; 5 in Figure 21). Possible paleogeomorphic and stratigraphic traps can form at unconformities due to burial of volcanic edifices, valley infill and contacts between reservoirs and seals deposited on the tephra flanks, with reservoirs pinching-out towards the

central crater (e.g. Bergman et al., 1992; Bischoff et al., 2017; 20 and 21 in Figure 21). Sub-vertical fluid migration can be controlled by igneous and tectonics fractures/faults (including intrusions of type-4 that cross-cut the base of syn-eruptive deposits, such as in the MVS), or by cooling fractures, by inclined tabular permeable deposits located on the tephra flank and tephra ring, and by cylindrical chaotic deposits of the central crater and diatremes (14, 22, 23 and 24 in Figure 21).

In summary, architectural elements of the constructional stage can form world-class hydrocarbon fields. Reservoirs in these fields can have high fluid deliverability towards 4-way closures due to the inclined flanks of cone-type volcanoes. These cones often show interbedded permeable and non-permeable rocks as part of the same structure (Bergman et al., 1992; Bischoff et al., 2017). The geometries and interconnectivity of these reservoir rocks are complex and may be difficult to predict.

Petroleum Elements of the Degradational Stage

Potential reservoirs formed during the degradational stage can be composed of debris deposits eroded from the volcanic edifices, which can include volcanic breccias and conglomerates, reworked carbonates, and non-volcanogenic siliciclastic coarse-grained deposits transported by submarine channels in association with the volcanic edifices (25 in Figure 21). Based on examples of the MVS, these deposits are most likely to be located in the central crater, tephra flank, and cone apron of cone-type volcanoes. Seals are mainly formed by fine-grained sedimentary deposits that drape the volcanoes (6 in Figure 21). Late hydrothermalism can induce both secondary porosity and cementation (Vieira de Luca et al., 2017; Lima and De Ros, 2019). Post-volcanic faults associated with differential compaction and subsidence can transport hydrocarbons to paleo-geomorphic and stratigraphic traps, and to permeable sedimentary deposits that dip away from and pinch-out against the volcanic edifice (20, 21 and 28 in Figure

21). In summary, there is some potential for hydrocarbon accumulation in architectural elements of the degradational stage, however, reservoirs are likely small, disconnected and localized.

Petroleum Elements of the Burial Stage

During the burial stage, sedimentary reservoirs can be impacted by the location of the volcanic structures. Sandstone reservoirs with 2.5 Mbbl of oil are reported to drape buried volcanoes in the Torch field, USA (Rives, 1968; apud Schutter, 2003). High-quality carbonate reservoirs can form on volcanic highs, with the potential to trap very large hydrocarbon volumes in 4-way closures associated with the volcanic structures during progressive burial (20 in Figure 21). Discoveries in Indonesia demonstrate that tropical carbonates located on volcanic structures have been a proven petroleum play since the 1970's. In offshore Sumatra, Krishna and Rama fields together produced 198 Mbbl from reefs and lagoon facies on the rim of volcanic islands. During lowstand cycles and exposure to freshwater conditions, original tight facies developed high secondary porosity due to leaching of aragonitic material (Wight and Hardian, 1982). In offshore Myanmar, the Yadana field is formed by shallow-water carbonate rocks build-up on a paleo volcanic high, and contains an estimated 7 TCF of gas (Paumard et al., 2017)

More recently, world-class accumulations discovered in offshore Brazil suggest that this play works in the pre-salt sequence of both South Atlantic conjugate margins. For example, the Pão de Açúcar field contains estimated values of 700 Mbbl of oil and 3 TCF of gas in carbonates and pillow-basalts located on the top of a volcanic edifice. Reservoirs of this field present abundant vugs, fractures, caverns, and patches of microporosity developed due to intense late hydrothermal alteration (Vieira de Luca et al., 2017). The Lula and Mero fields together have a reserve estimated of > 10 Gbbl. Reservoirs of these fields are composed of carbonates deposited on volcanic-siliciclastic rift sequences associated to structural highs (e.g. Mohriak, 2008; Carlotto et al., 2017). The role of the syn-rift volcanic structures on the formation of carbonate reservoirs remain unclear and will need to be unravelled by future work.

In the South Island of New Zealand, outcrop observations from the Waiareka-Deborah monogenetic volcanic field suggest that these clusters of volcanoes can create localized highs of >225 km^2. Above these structures, high energy currents winnow micrite and cause fragmentation of cool-water bioclasts (Thompson et al., 2014). Aragonitic components underwent dissolution at the seafloor and the lack of cements/matrix produce a clean bryozoan grainstone ca 50 m thick, and porosity above 50% before deep burial (Thompson et al., 2014). Offshore the Canterbury and Taranaki basins, seismic surveys and borehole indicate that there are many Meso-Cenozoic monogenetic fields and large polygenetic volcanic complexes, potentially associated with overlaying carbonates and commonly forming 4-way closures due to burial doming (Barrier et al., 2017; Bischoff et al., 2018).

In summary, very large (> 1Gbbl) hydrocarbon accumulations can form in association with architectural elements of the burial stage, mainly in paleogeographic traps located at the top of buried volcanoes. Volcanic structures can provide ideal conditions for the deposition of sedimentary rocks (mainly carbonates) with high quality reservoir properties. These rocks are likely entrapped in large 4-way closures due to progressive burial and differential compaction across the volcanic edifice.

Conceptual Intrusion-Related Hydrothermal Systems in Monogenetic Fields

Petroleum and geothermal systems share many similarities. Both systems rely on the presence of fundamental elements and processes to form a prolific prospect. Similarly to the concept of petroleum system (Magoon and Dow, 1994), the introduction of a unifying concept to assess the economic potential of geothermal systems can help to reduce the risk of prospects, and can increase the chances of finding valuable energy resources in association with igneous activity. Key elements and processes for geothermal systems are: a source of heat (typically magma or hot igneous rocks), a reservoir body (which can be fractured or porous), water (vapour or liquid), and a permeable network to transfer fluids and heat through the system (e.g. Goff and Janik,

1999; Stimac et al., 2015; Sydnes et al., 2017). Magma emplaced in sedimentary basins can provide these conditions and form hydrothermal systems that are prolific producers for geothermal energy (Jiachao, 2012; Iyer et al., 2013; Procesi et al., 2019). Understanding the distribution and impact of intrusions within the basin strata are important for assessing the fundamental elements and processes that determine if intrusion-related hydrothermal systems are to exist. Intrusion-related hydrothermal systems can form when a shallow magmatic intrusion emplace within sedimentary rocks that contain a permeable network for hot water circulation (e.g. Procesi et al., 2019). These systems are considered the hottest (220° to 350°C) and most prolific producers for geothermal energy (Stimac et al., 2015). Basaltic intrusions in sedimentary basins (e.g. MVS) usually have high temperatures in which melts are estimated to be $> 1100^{o}$ C (e.g. Grove and Till, 2015; Aarnes et al., 2015).

In this section we explore the analysis of architectural elements of the MVS to identify potential impacts on hydrothermal systems related to shallow intrusions in sedimentary basins. The diverse plumbing-types of the MVS comprise architectural elements that vary in relation to the geometries of intrusive bodies, their sizes and volumes, architecture, and level of emplacement in different types of host rocks. These variations create situations that can impact hydrothermal systems, mostly related to (i) fluid migration pathways within the system, (ii) location of potential prospective zones, and (iii) changes in the composition of fluids due to interaction with host rocks (Figure 22).

Due to their large dimensions, saucer-shaped sills (plumbing-type 1) are likely the most prolific type of intrusion in MVS-type modern volcanic field (Figure 22). These intrusive bodies have volumes estimated to be up to 2.5 km^3 for individual sills. The emplacement of these intrusions is associated with a ring-shaped network of faults and fractures in the overburden strata that accommodate deformation (e.g. Hansen and Cartwright, 2006; Gallant et al., 2018). Flow models presented in Iyer et al. (2013) show that the merging of fluids from near saucer-

intrusions could result in hydrothermal plumes located at the lateral edges of the sills. Based on laboratory experiments, Montanari et al. (2017) argue that these fracture and fault networks could influence the formation of potential prospects for supercritical geothermal fluids. In the MVS, the tips of the inclined sheets of saucer-intrusions (5 and 8 in Figure 22) correspond to the transition between plumbing-type 1 and 3. This transition is characterised by a strong sub-vertical network of faults and fractures, where fractures and faults could be a prospective zone for directly tapping into magmatic heat by drilling into or near shallow intrusive bodies (e.g. Stimac et al., 2015). These sub vertical fracture networks can conduct magma upwards and feed eruptions at the surface, or facilitate outflowing of fluids to hydrothermal vents and fumaroles (e.g. Holford et al., 2012; Planke et al., 2005; Blanke, 2012; Jackson, 2012; McLean et al., 2017; 6 in Figure 22). Faults and fractures may create pathways for surface water to recharge the system, which can favour the formation of hydrothermal convection cells (13 in Figure 22).

Plumbing-type 2 are usually shallow (< 500 m deep) and individual intrusions that have smaller volumes (up to 0.05 km^3) than saucer-sills, however, they are typically characterised by a complex intrusive network with dozens (maybe hundreds) of intrusions. Their association with fractures and disrupted blocks may favour contact with surface water and development of a liquid-dominated open system (4 in Figure 22). In rare cases they may form a system isolated from groundwater, in which steam-dominated conditions may prevail (Stimac et al., 2015). Plumbing-types 4 and 5 show small and isolated intrusions and have little potential to form economic intrusion-fed geothermal systems (Figure 22). Clay caps are more likely to form at shallow levels due to alteration of volcanic rocks with high glass and plagioclase content, rather than in siliciclastic and carbonate pre-magmatic sequences, which could maintain the life spans of these systems (e.g. Stimac et al., 2015; 17 in Figure 22). As a rule-of-thumb for all plumbing types, geothermal systems hosting intrusions and reservoirs in carbonates are likely to be enriched in CO_2, while systems hosted in organic-rich rocks are potentially enriched in CO_2,

CH$_4$, and H$_2$S (e.g. Goff and Janik, 1999; Deegan et al., 2010; Iacono-Marziano et al., 2013; Aarnes et al., 2015; Robertson et al., 2015; Arnórsson et al., 2015; 2 and 3 in Figure 22).

Conclusions

Reconstruction of the architecture of the Maahunui Volcanic System enables us to understand how igneous and sedimentary architectural elements interact and are distributed in time and space, due to the emplacement of magma, construction of a volcanic sub-sea morphology, degradation and burial of a monogenetic volcanic field in a sedimentary basin. The MVS plumbing system comprises of mainly saucer-shaped sills, sills and dike swarms and minor laccoliths, distributed systematically into five plumbing-types, which have been characterised according to their level of emplacement and spatial relationship to each other, and to host sedimentary strata. Saucer-sills emplaced at ca 1000 m depth in paralic to marine sedimentary strata are likely to have fed many MVS eruptive vents. The extrusive part of the volcanic field was erupted entirely in a deep marine setting (ca 1000 m water depth) and contains at least 31 deep-water equivalents to crater-type (i.e. maar-diatreme volcanoes), as well as cone-type volcanoes (i.e. tuff cones). Crater-type volcanos have 8 main syn-eruptive architectural elements: root zone, lower and upper diatreme, tephra ring and tephra plain, intra-crater cones, overspill wedge and tephra fallow carpet. Cone-type volcanoes have five main syn-eruptive architectural elements: basal cone, central crater, tephra flank, cone apron and tephra fallout carpet. Each of these elements have been formed by a combination of eruptive and associated sedimentary deposits, with minor and localized intrusions. After volcanism ceased, processes of degradation and burial of the volcanic edifies strongly impacted local sedimentation for at least ca 6 Ma after the volcanoes ceased to erupt, and ca 1 Ma after they were completely buried. Degradation and burial of the volcanic edifices of MVS produced five main sedimentary architectural elements (i.e. inter-cone plains, epiclastic plumes, canyons and gullies, burial domes and seamount-edge fans). The complete characterisation of the architecture of the MVS allows us to understand how

certain combinations of volcanic and sedimentary architectural elements can form hydrocarbon leads and possible geothermal systems in association with volcanoes buried in sedimentary basins. At the endogenous level, intrusions and magmatic deformation can create fractured reservoirs, seals, structural traps, and pathways to sub-surface fluid percolation. Large saucer-sills and intrusion swarms have the potential to host significant oil and gas accumulations, and can produce high-temperature intrusion-related geothermal systems. Both petroleum and geothermal systems are likely to be enriched in CO_2 if the intrusions are emplaced in carbonate rocks, or are likely to be enriched in CO_2, CH_4, and H_2S if the intrusions interact with organic-rich host rocks. At the exogenous level, a complex network of eruptive and sedimentary deposits can form substantial hydrocarbon fields due to high fluid deliverability towards 4-way closures, which can be sealed if the volcanic structures are buried in fine-grained marine sediments or evaporitic rocks. Progressive burial of the volcanoes can create ideal conditions for the formation of high-quality carbonate reservoirs located above buried volcanic structures. Differential compaction between the volcanic structures and enclosing sedimentary rocks can entrap these carbonate reservoirs in large 4-way closures, with potential to host world-class (> 1Gbbl) hydrocarbon fields. Understanding the relationship of diverse architectural elements, their petrophysical properties, and post-formational events that can change their original characteristics is important to assess the risks and to improve the likelihood of finding commercially viable geoenergy resources in association with buried and active monogenetic volcanic systems.
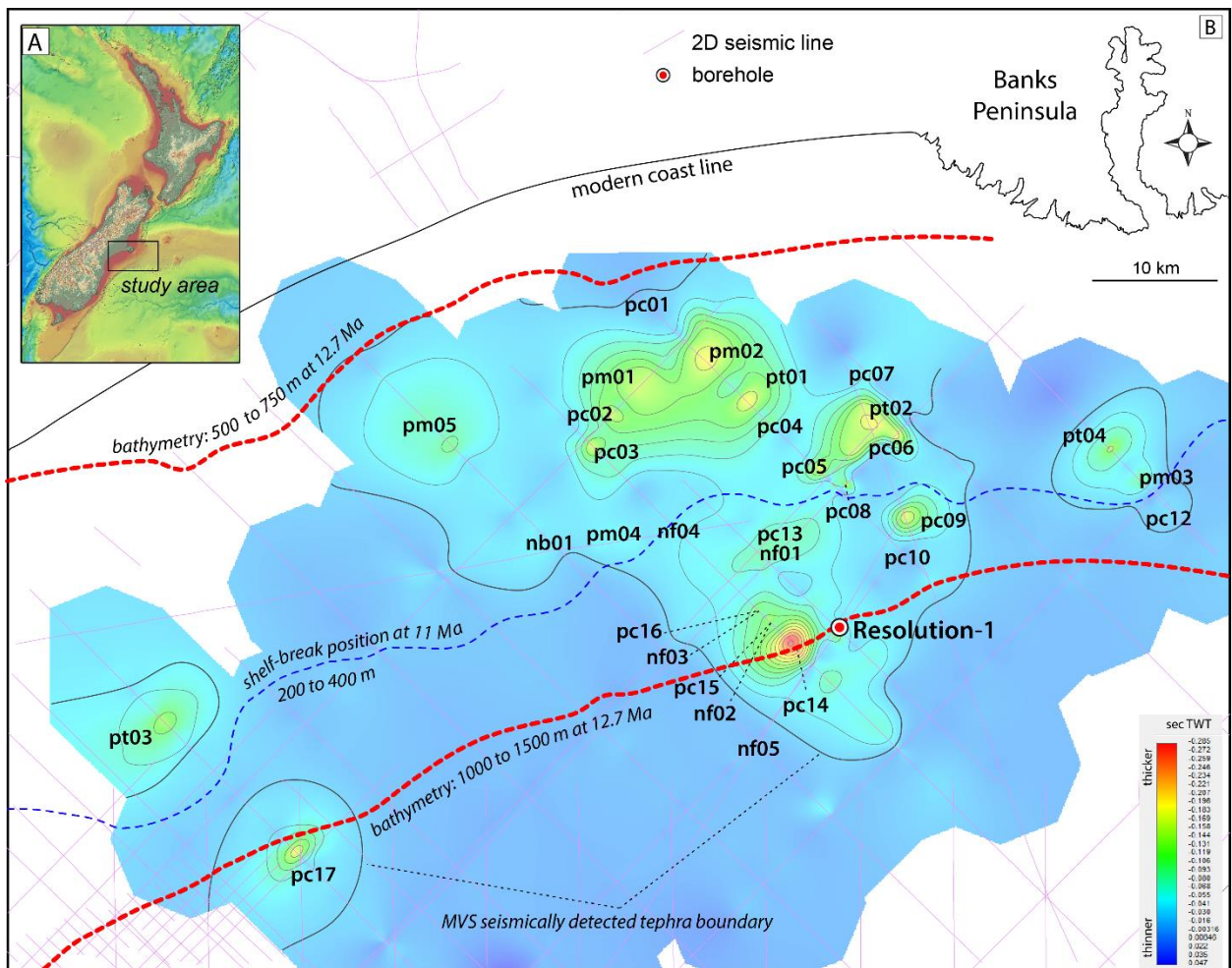
Figure 1: A) Location of the study area over the New Zealand topographic and bathymetric map (from Petroleum Exploration 2018 datapack). B) Paleogeographic map of the Maahunui Volcanic System. Abbreviations are plotted at the position of MVS volcanoes and correspond to their morphology. Pc's (positive cone), pt's (positive trapezium), pm's (positive mounds) represent cone-type volcanoes. Nf's (negative funnel-like) and nb's (negative basin-like) correspond to crater-type volcanoes. Red dashed lines show the approximate bathymetry at the onset of eruptions in the MVS. Blue dashed line shows the position of the shelf-break at 11 Ma. (Modified from Bischoff, 2019).
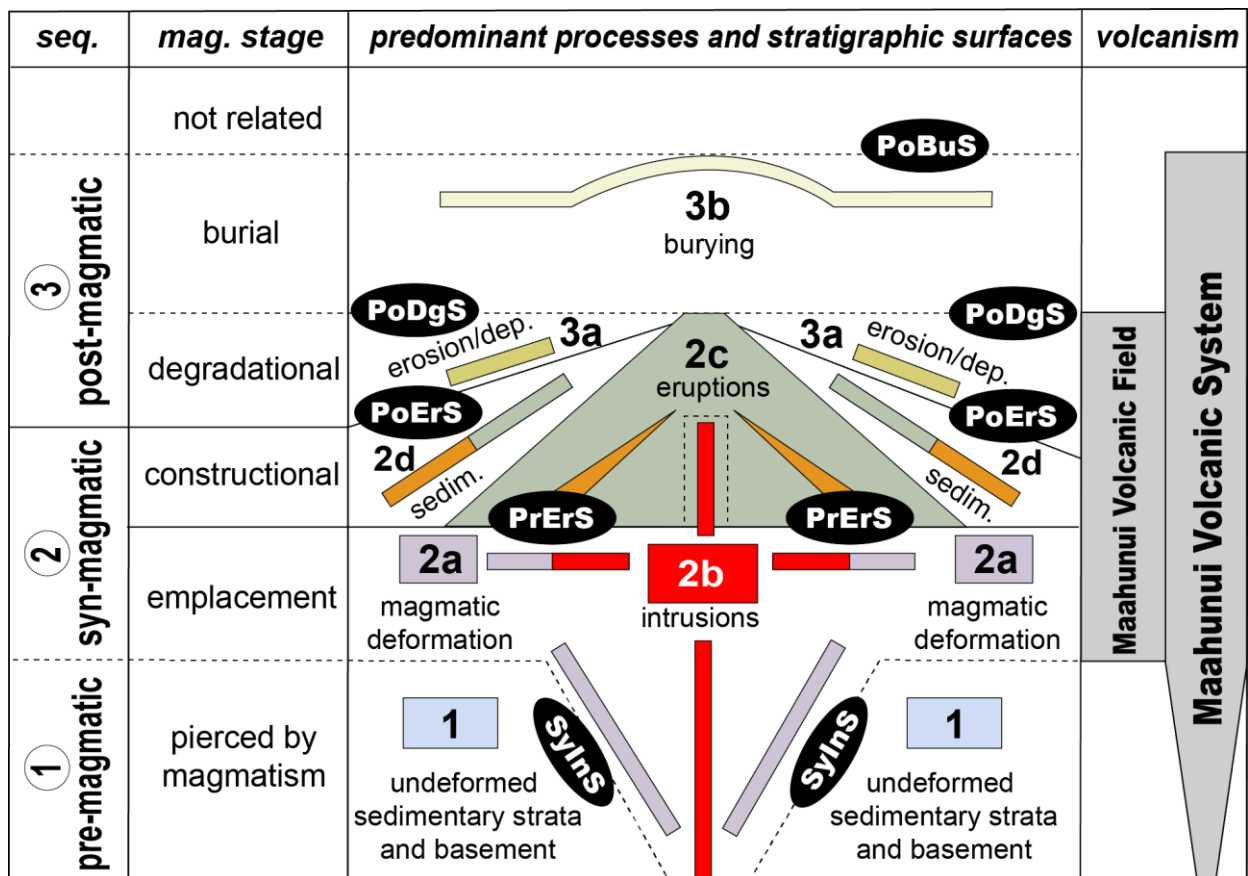
Figure 2: Conceptual representation of the magmatic sequences and stages (left), predominant geological processes, stratigraphic surfaces (centre), and boundaries of MVF and MFS (right).

input

seimic image from the study area

it was sampled by borehole well? — *no* → **2D seimic characterization**

internal and external reflectors configuration
reflectors terminations
2D morphology of reflectors
relationship to surrounding strata
2D bounding surfaces

yes

integration

petrographic characterization

2 mm

0.5 mm

1D lithofacies distribution, processes, products, chemistry, absolute and relative age

2D geological interp.

well

monzogabbro intrusion
75 m thick
5 km lateral extension
U shaped
emplaced in paralic rocks

2D seimic interpretation

high amplitude reflector
thickness unknown
5 km lateral extension
U shaped
cross-cut parallel reflectors

there is 3D seismic data available or it is possible to map 3D geobodies from the 2D dataset?

yes   *no*

3D seimic characterization

3D geobody geometry
contact relationship of geobodies
3D bounding surfaces

analogy to 3D interpretation elsewhere

Kora Volcano, Taranaki Basin. Bischoff et al., 2017

analogy to world-wide outcroping systems

Inclined sheets

Golden Valley Sill

Galland et al., 2018. Photo: Stéphane Polteau

Inner sill

Karoo Basin, Africa

insights into 3D facies architecture, possible processes and products

with well data   **output**   *without well data*

tested element

Saucer-shaped intrusion of basaltic composition and middle Miocene age, varying in size from tens of meters thick to kilometres wide, bounded by sharp contacts between igneous and sedimentary rocks, which are commonly observed in sedimentary basins pierced by hypabyssal intrusions.

untested element

Saucer-shaped anomaly cross-cutting parallel reflectors (intrusion?) of unknown composition and younger then Paleocene (relative age), varying in size from unknown thickness to kilometres wide, bounded by the external contact of a high impedance rock body, which are commonly associated to hypabyssal intrusions in sedimentary basins.
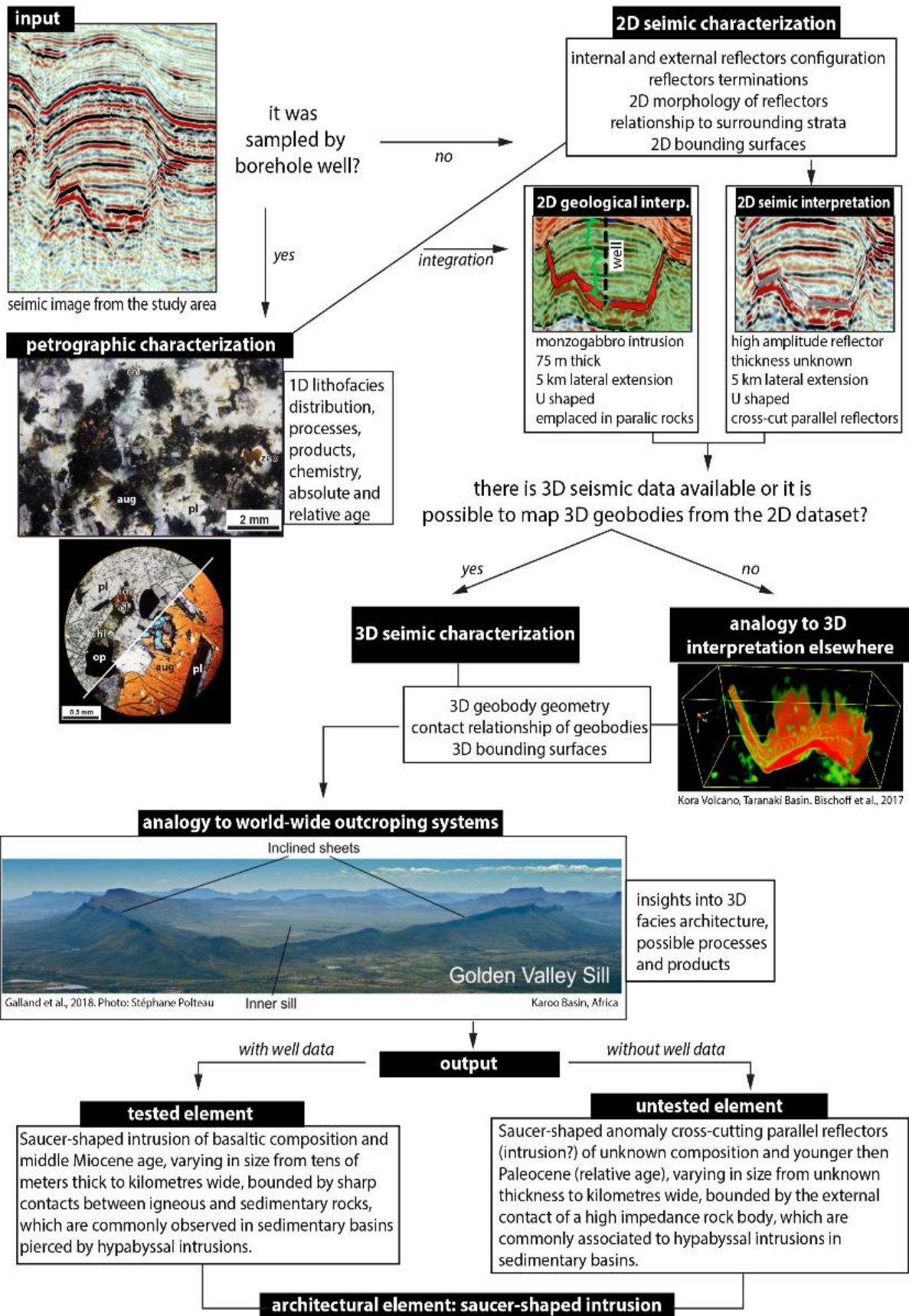
architectural element: saucer-shaped intrusion

Figure 3: Methods used for the identification and interpretation of volcanic and sedimentary architectural elements in the MVS. The input 2D seismic reflection are described and compared with analogues. Elements sampled by drill holes can provide an accurate geological characterisation of the anomaly, while interpretation without physical confirmation remains only hypothetical.
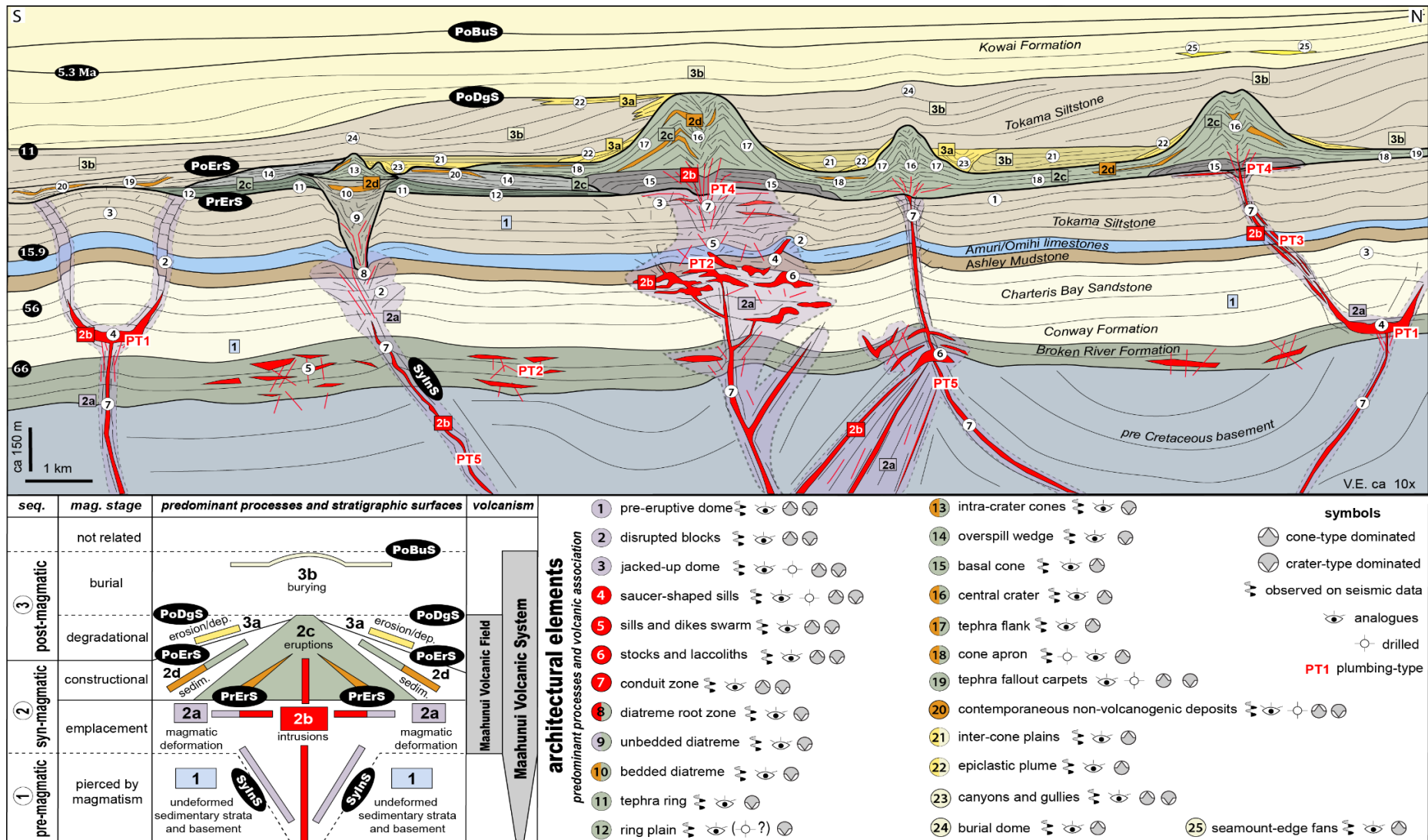
Figure 4: Schematic representation of the stratigraphic sequences and surfaces, magmatic stages, architectural elements, and predominant processes associated with MVS. Numbers in circles represent the location of the architectural elements indicated in the key. Numbers in squares indicate the predominant processes in the key. The symbols in the right hand corner illustrate the database used for interpretations. Conduit zones and dikes have lateral thicknesses exaggerated for visualization proposes. In this framework, PoDgS and PoBuS are related to the volcano in the centre of the figure. Lateral variation of the lithostratigraphic units are not shown in the image. The pre-eruptive dome is a regional feature shown in Figure 10.

47
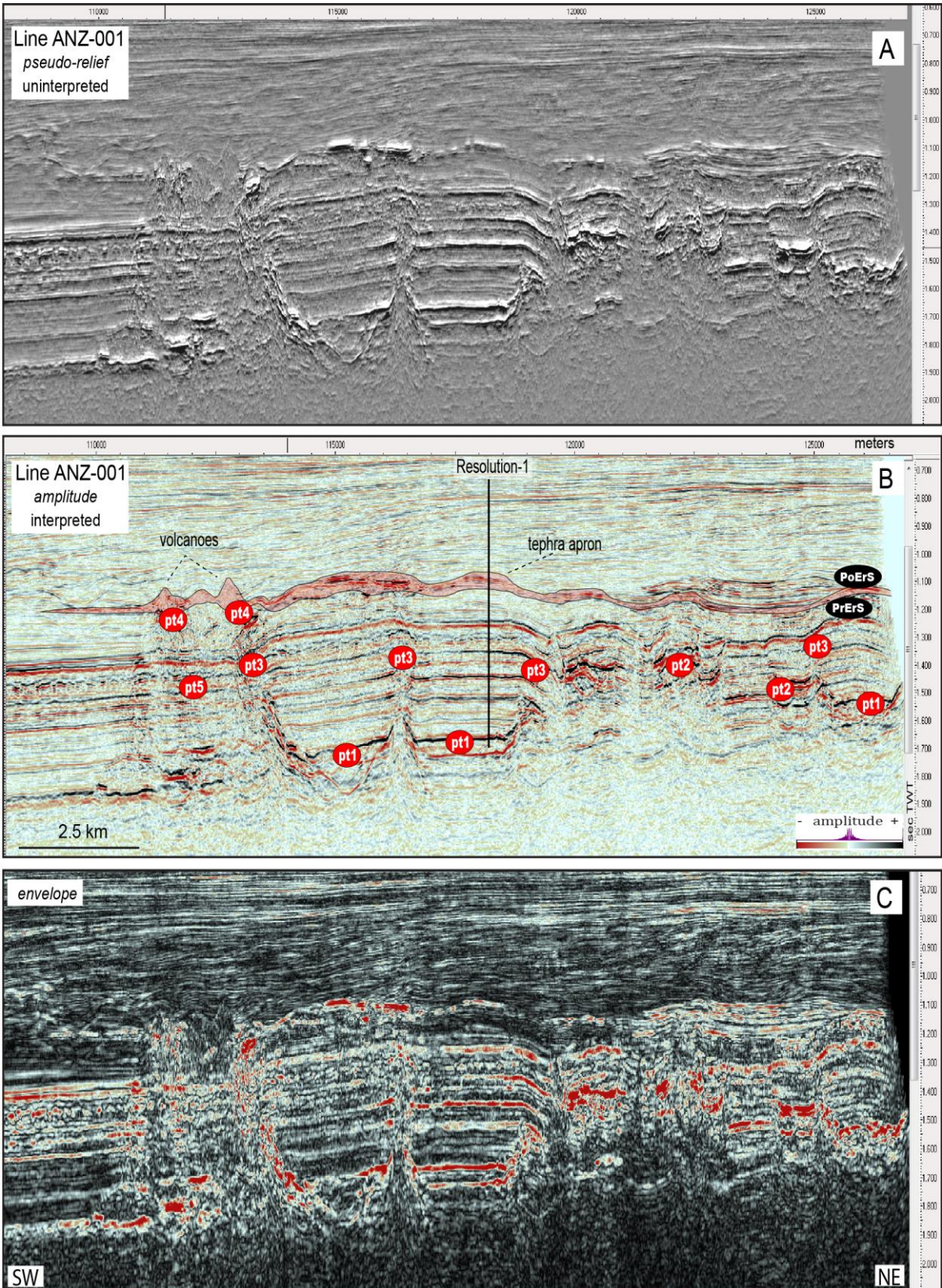
Figure 5: 2D seismic reflection lines showing the locations and geometries of the five plumbing-types observed in the MVS. Images A, B and C for the same line ANZ-001 which display the seismic attributes pseudo-relief (A), amplitude (B) and envelope (C). Note the systematic vertical distribution from type-1 (deeper) to type-4 (shallower) and their relationship. Type-5 differs from the other types in that it represents a deep source-to-surface feeder system.
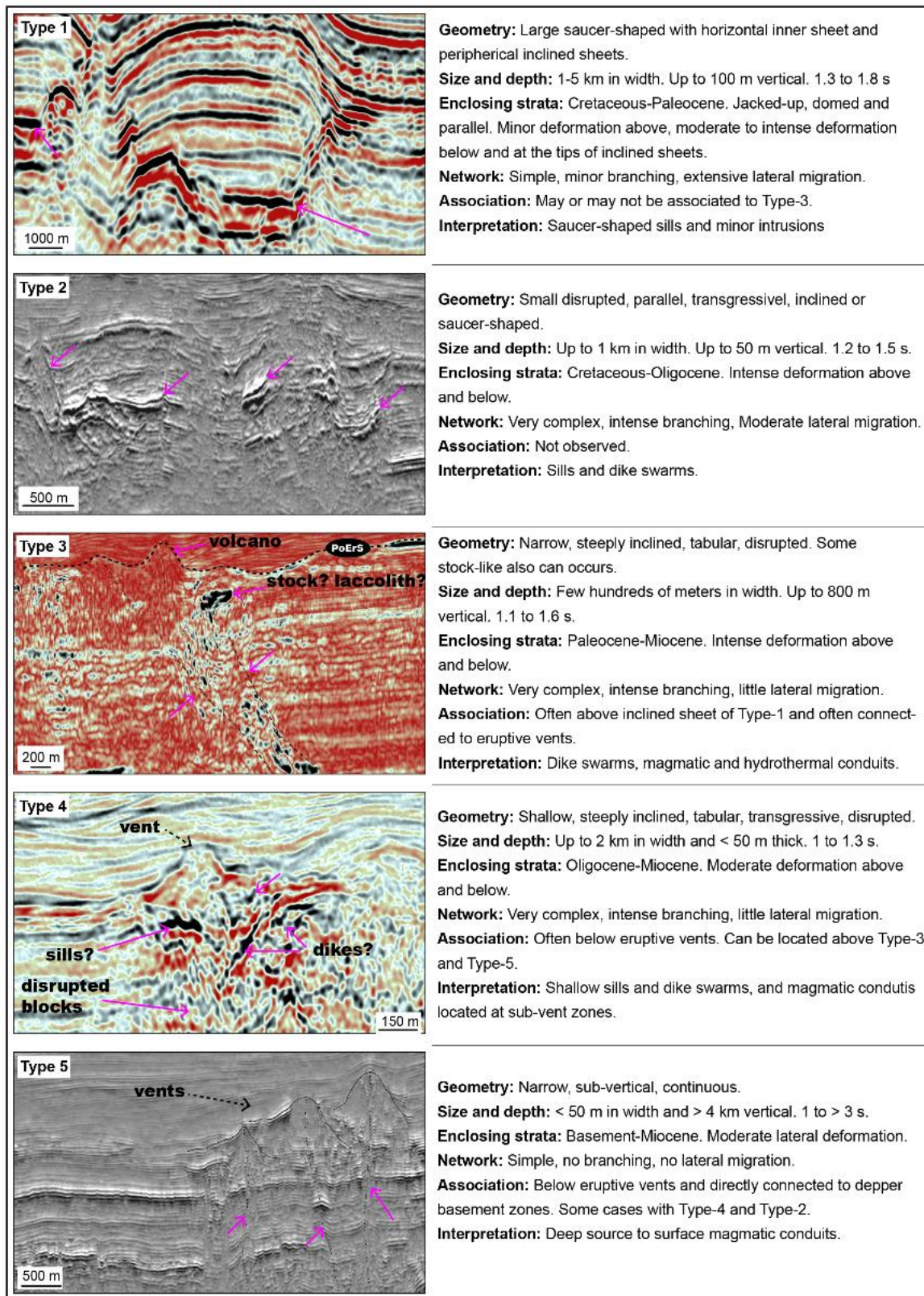
Type 1

1000 m

Geometry: Large saucer-shaped with horizontal inner sheet and peripherical inclined sheets.
Size and depth: 1-5 km in width. Up to 100 m vertical. 1.3 to 1.8 s.
Enclosing strata: Cretaceous-Paleocene. Jacked-up, domed and parallel. Minor deformation above, moderate to intense deformation below and at the tips of inclined sheets.
Network: Simple, minor branching, extensive lateral migration.
Association: May or may not be associated to Type-3.
Interpretation: Saucer-shaped sills and minor intrusions

Type 2

500 m

Geometry: Small disrupted, parallel, transgressivel, inclined or saucer-shaped.
Size and depth: Up to 1 km in width. Up to 50 m vertical. 1.2 to 1.5 s.
Enclosing strata: Cretaceous-Oligocene. Intense deformation above and below.
Network: Very complex, intense branching, Moderate lateral migration.
Association: Not observed.
Interpretation: Sills and dike swarms.

Type 3

volcano   PoErS

stock? laccolith?

200 m

Geometry: Narrow, steeply inclined, tabular, disrupted. Some stock-like also can occurs.
Size and depth: Few hundreds of meters in width. Up to 800 m vertical. 1.1 to 1.6 s.
Enclosing strata: Paleocene-Miocene. Intense deformation above and below.
Network: Very complex, intense branching, little lateral migration.
Association: Often above inclined sheet of Type-1 and often connected to eruptive vents.
Interpretation: Dike swarms, magmatic and hydrothermal conduits.

Type 4

vent

sills?   dikes?

disrupted blocks

150 m

Geometry: Shallow, steeply inclined, tabular, transgressive, disrupted.
Size and depth: Up to 2 km in width and < 50 m thick. 1 to 1.3 s.
Enclosing strata: Oligocene-Miocene. Moderate deformation above and below.
Network: Very complex, intense branching, little lateral migration.
Association: Often below eruptive vents. Can be located above Type-3 and Type-5.
Interpretation: Shallow sills and dike swarms, and magmatic condutis located at sub-vent zones.

Type 5

vents

500 m

Geometry: Narrow, sub-vertical, continuous.
Size and depth: < 50 m in width and > 4 km vertical. 1 to > 3 s.
Enclosing strata: Basement-Miocene. Moderate lateral deformation.
Network: Simple, no branching, no lateral migration.
Association: Below eruptive vents and directly connected to depper basement zones. Some cases with Type-4 and Type-2.
Interpretation: Deep source to surface magmatic conduits.

Figure 6: 2D seismic reflection images and characterisation of the five plumbing-types from the MVS. Seismic attributes of the images are: Type-1= amplitude, Type-2= pseudo-relief, Type-3= envelope, Type-4= amplitude and Type-5= pseudo-relief.

49

Figure 7: Macroscopic photograph of a sample from the Resolution-1 core at the depth of 1663 m (A) showing augite (aug), plagioclase (pl), acicular crystals of zeolite (zeo), and miarolitic cavities (mia). Thin-section in cross-polarized light (B) and plain light (C) showing augite and plagioclase with ophitic texture. Op are opaque minerals.
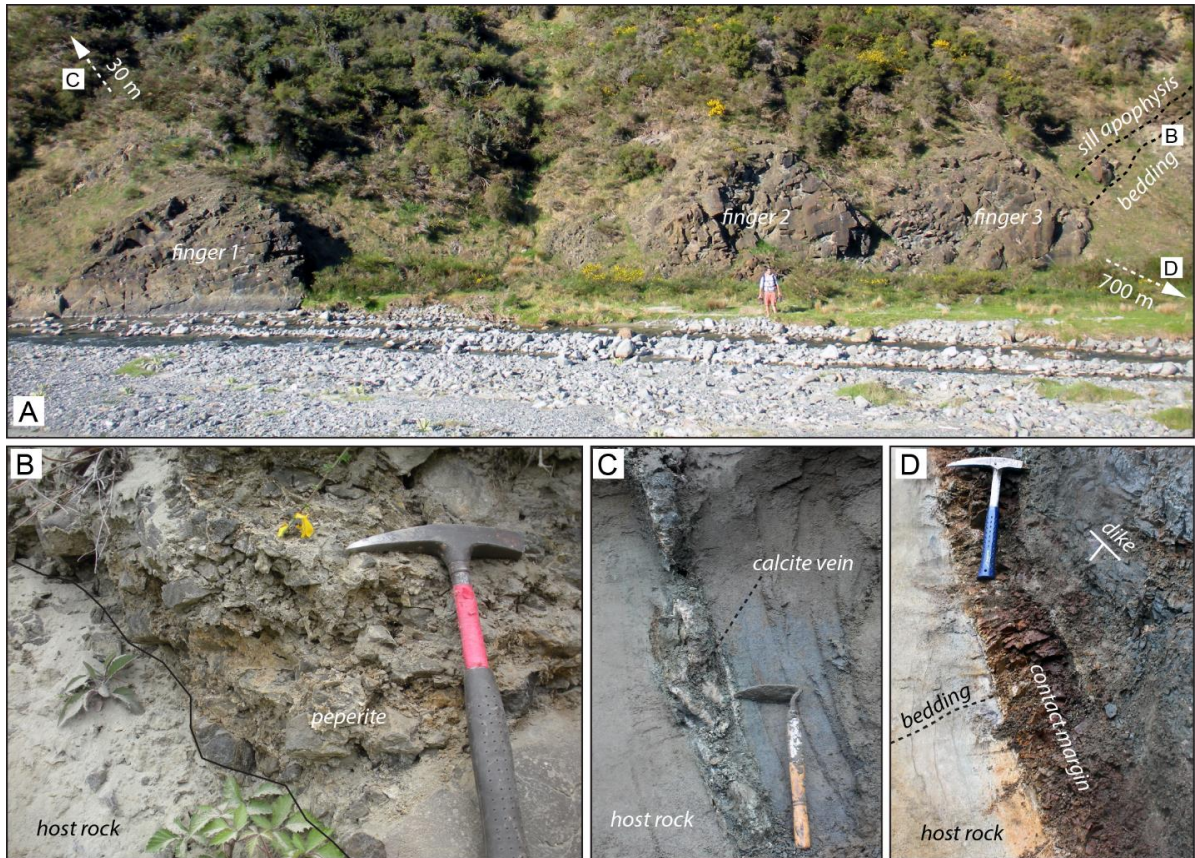
Figure 8: Photographs of potential analogue dikes outcropping in the Canterbury Basin. Intrusions have different patterns and products according to their depth of emplacement. At deeper levels, dikes show sharp contacts and little branching into enclosing sediments (D), while at shallower levels, they show magma finger terminations and several thin apophysis with peperitic borders. Thirty meters above the shallower intrusions, calcite veins (C) suggest migration of fluids up-sequence.
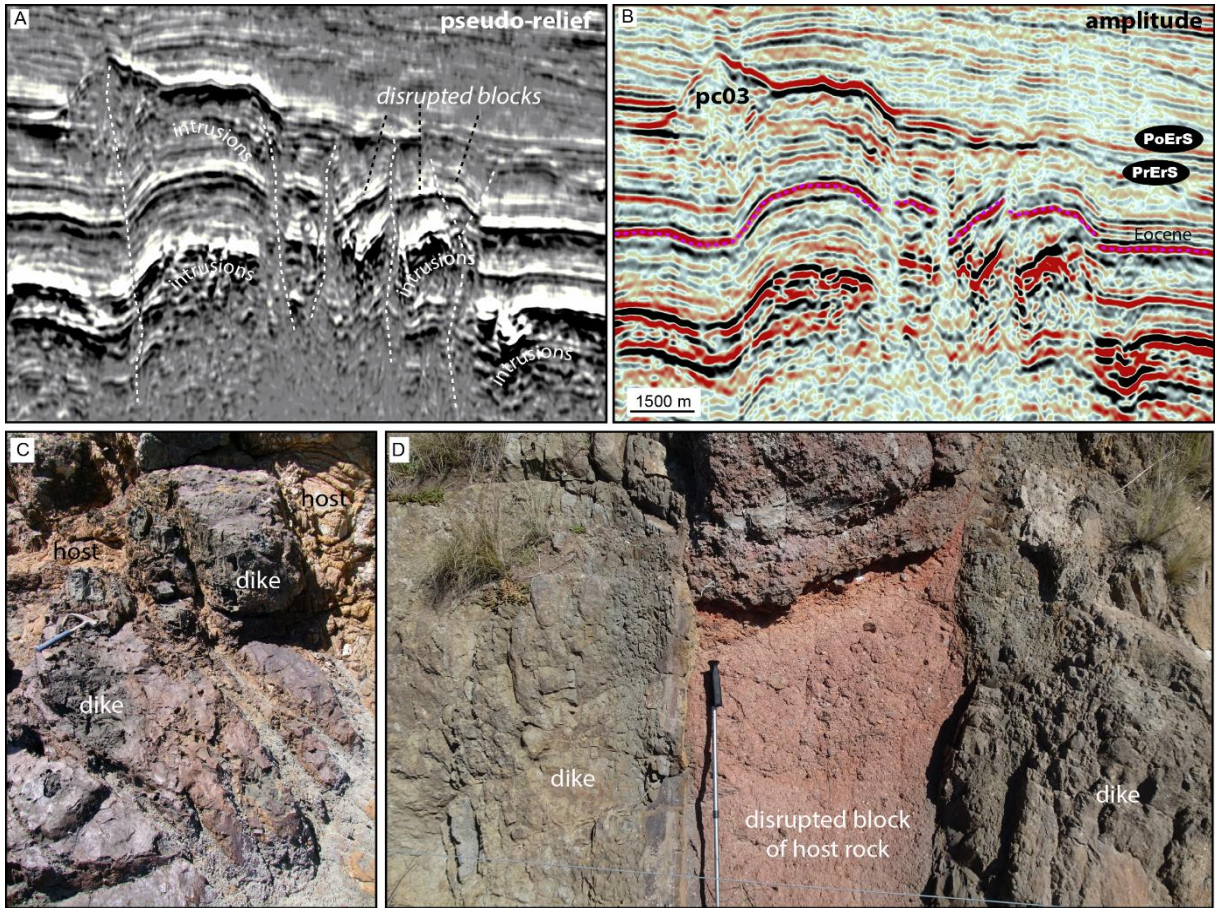
Figure 9: 2D seismic images (A and B) of disrupted blocks, and a possible outcrop scale analogue (C and D) of this architectural element in Banks Peninsula formed by host pyroclastic deposits cross-cut by multiple dike intrusions.
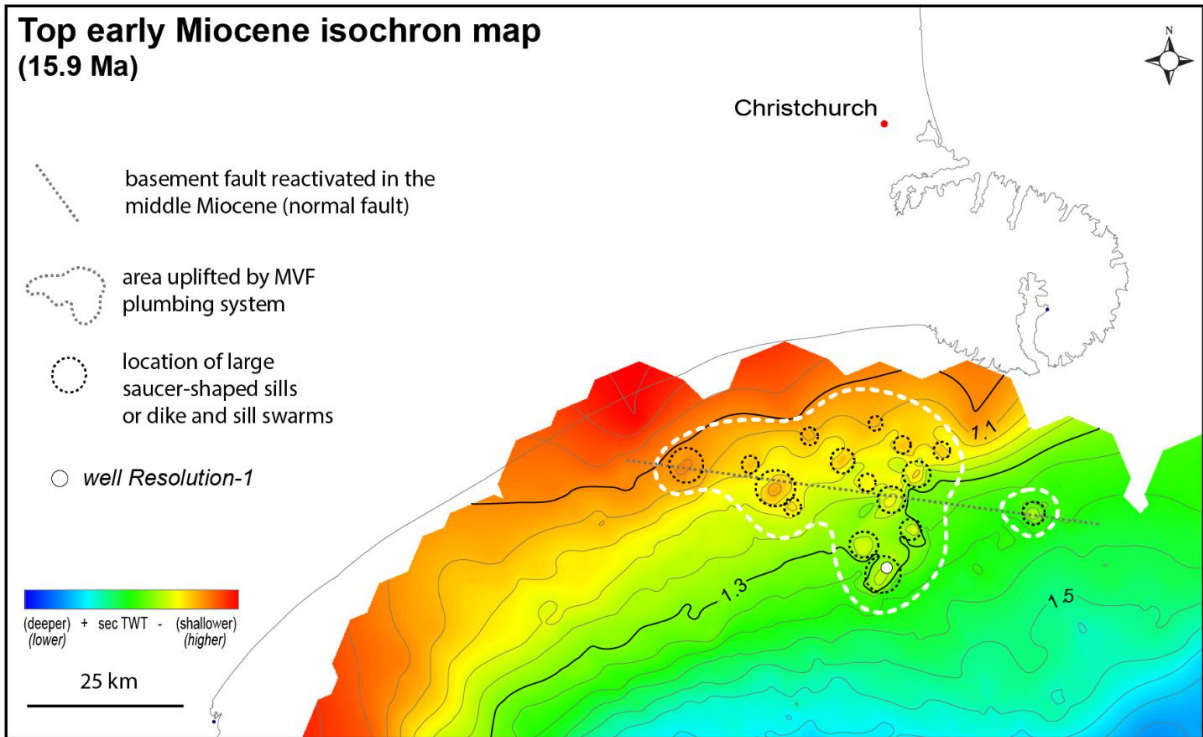
Figure 10: Top early Miocene isochron map of the northern part of Canterbury Basin. The area inside the white dashed line shows uplift with maximum vertical relief of ca 100 meters, coincident with the location of large sill and dike and sill swarms of the MVS plumbing system.
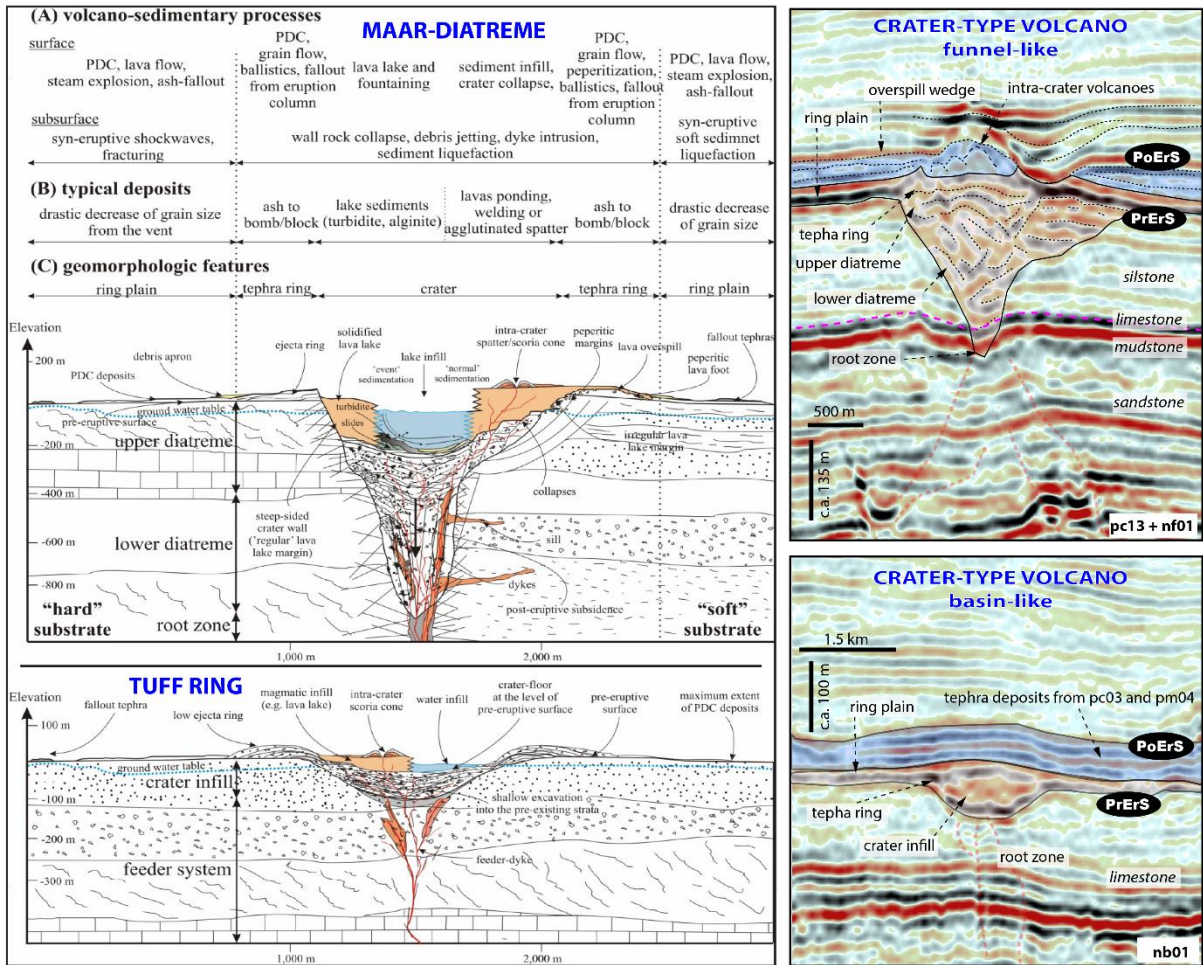
Figure 11: Images on the left hand side show a schematic cross-sections through a maar-diatreme and a tuff ring, and their typical volcano-sedimentary processes, deposits and geomorphologic features (from Kereszturi and Németh, 2013). On the right-hand side are shown interpreted 2D seismic lines of the MVS crater-type volcanoes, and their main large scale architecture.
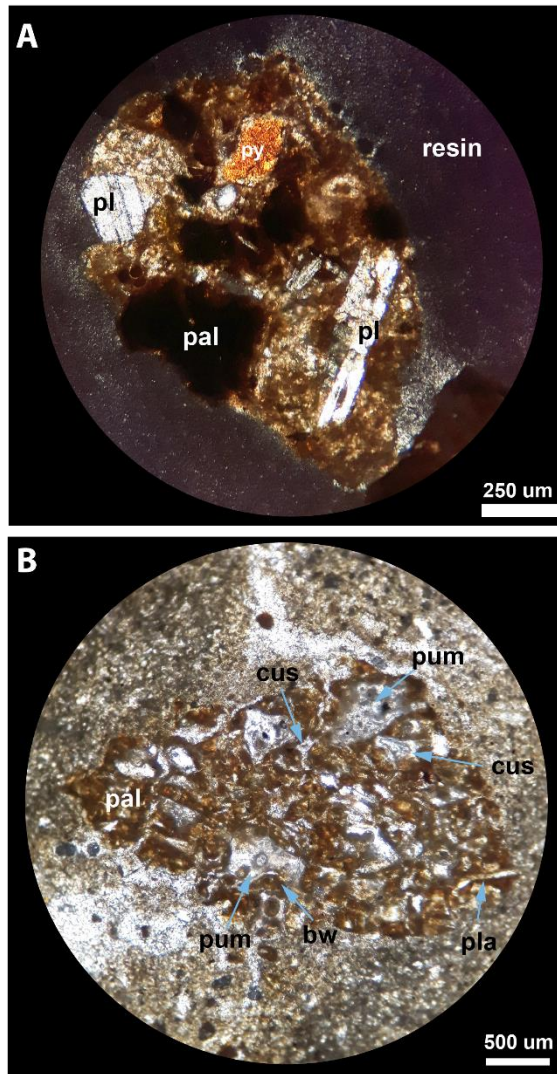
Figure 12: A) photographs in cross-polarized thin-section of volcanic rocks of MVS showing microporphyritic and vitrophyric textures, composed of plagioclase (pl), pyroxene (py) and pervasive palagonite (pal) alteration. B) Photograph of thin-sections in plain light showing a palagonite (pal) ground mass associated with glassy shards with cuspate (cus), platy (pla) and pumice (pum) shapes, and relics of bubble walls (bw).
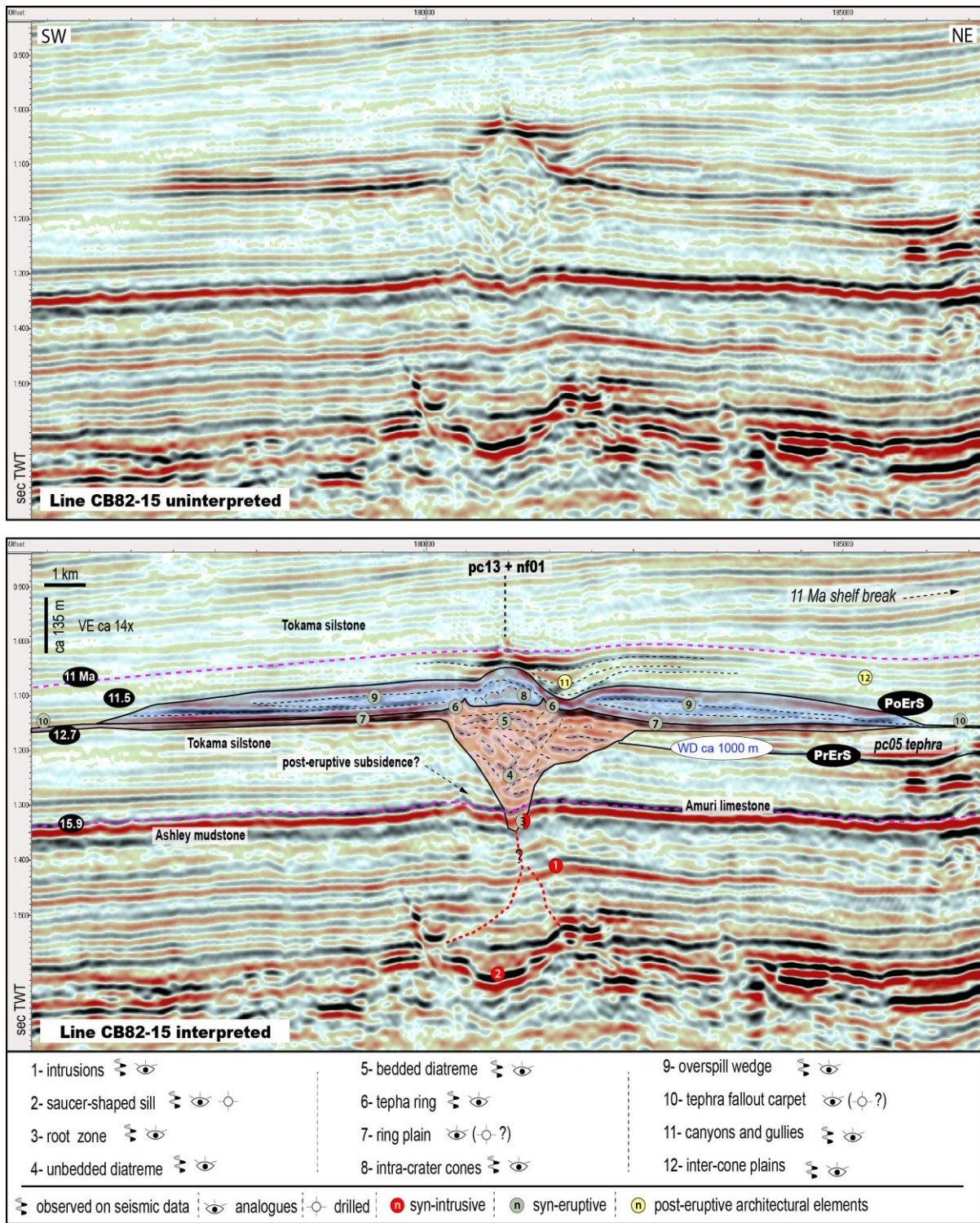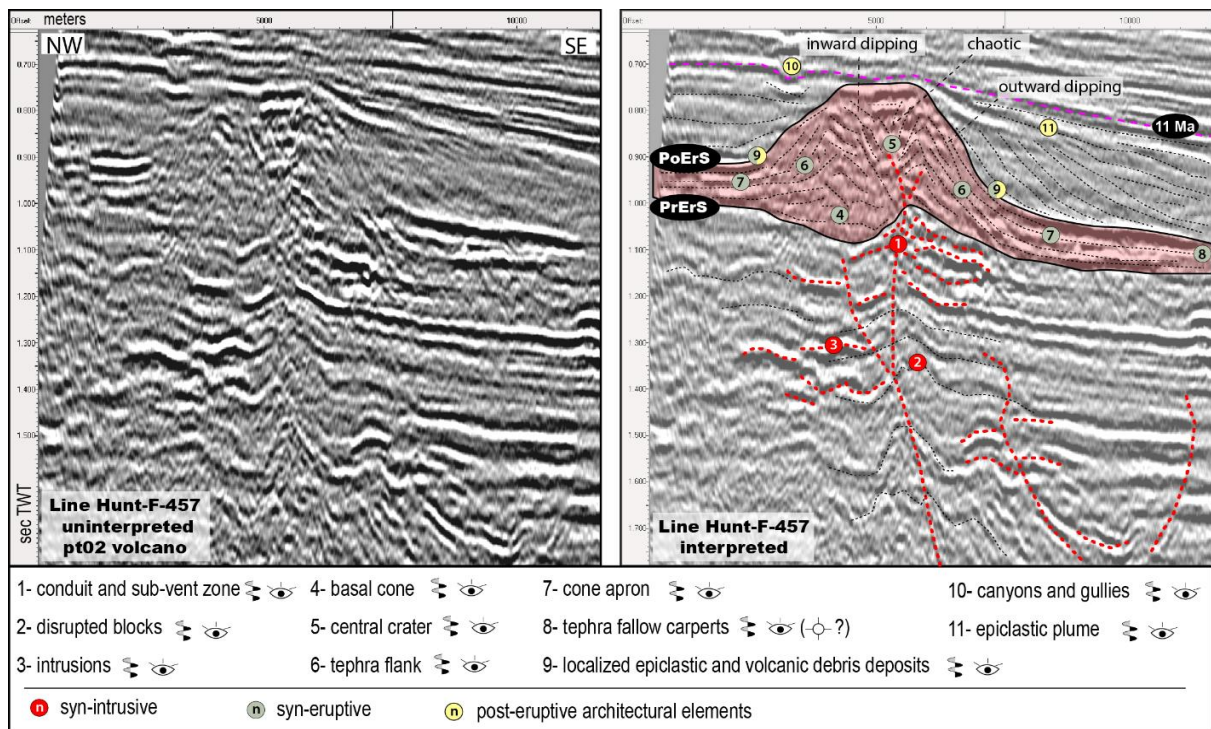
Figure 13: Uninterpreted (above) and interpreted (below) 2D seismic line showing the main architectural elements related to crater-type volcanoes in the MVS. Numbers in red circles are syn-intrusive architectural elements, in green syn-eruptive, and in yellow post-magmatic architectural elements. We observe that crater-type volcanoes present two distinctive morphologies related to at least two different eruptive-styles: lower part (in red) shows funnel-like excavation into PrErS and lateral high amplitude parallel reflectors, which we interpret to represent a submarine equivalent of a maar-diatreme volcano, and may be related to large subaqueous phreatomagmatic eruptions. Upper part (in blue) shows cone-like morphology and lateral semi-continuous reflectors in wedge-shape, which we interpreted as intra-crater volcanoes formed by late eruptive events, and associated material that overspills from the rim of the underlying maar-diatreme structure. WD is the interpreted approximate water-depth at the time of the formation of the volcanos.
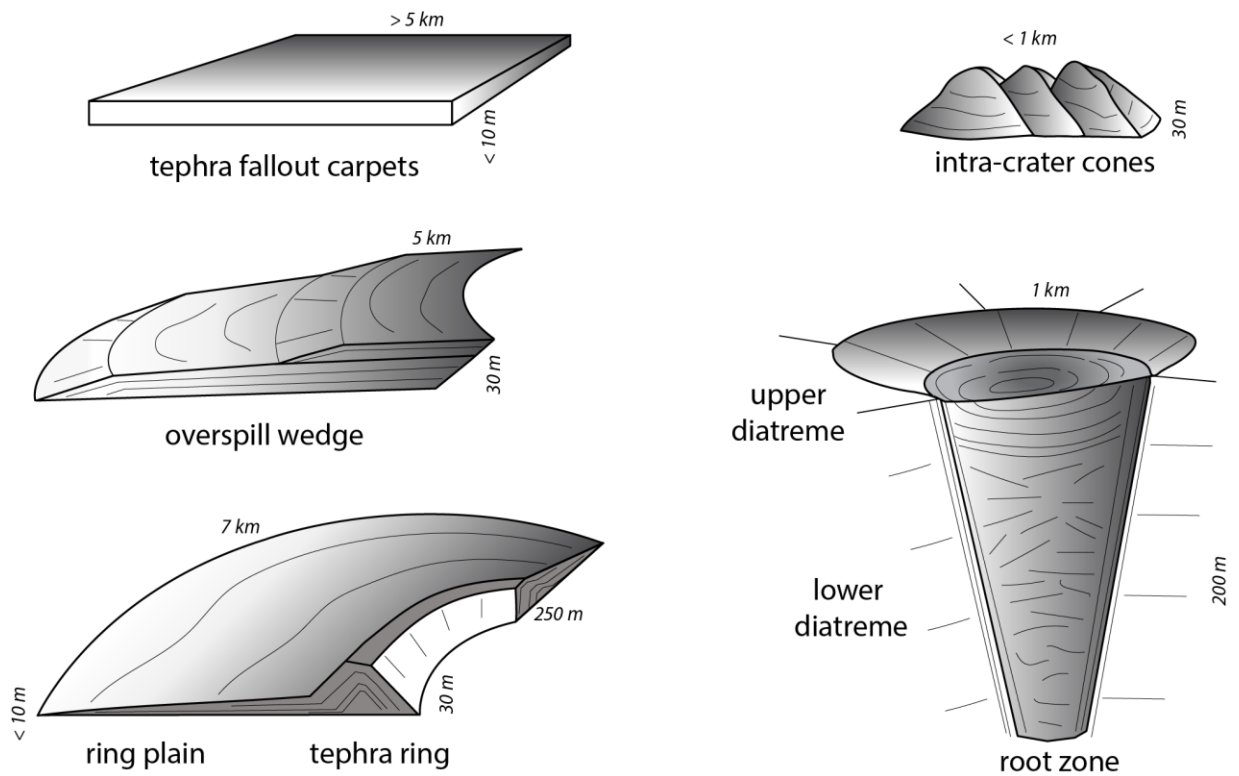
Figure 14: Three-dimensional representation of the main syn-eruptive architectural elements of crater-type volcanos of the MVS and their average size. Each of these large-scale elements can be composed by sets of smaller-scale elements formed by the interplay of volcanic activity, external receptor environments, and concomitant sedimentation.

57
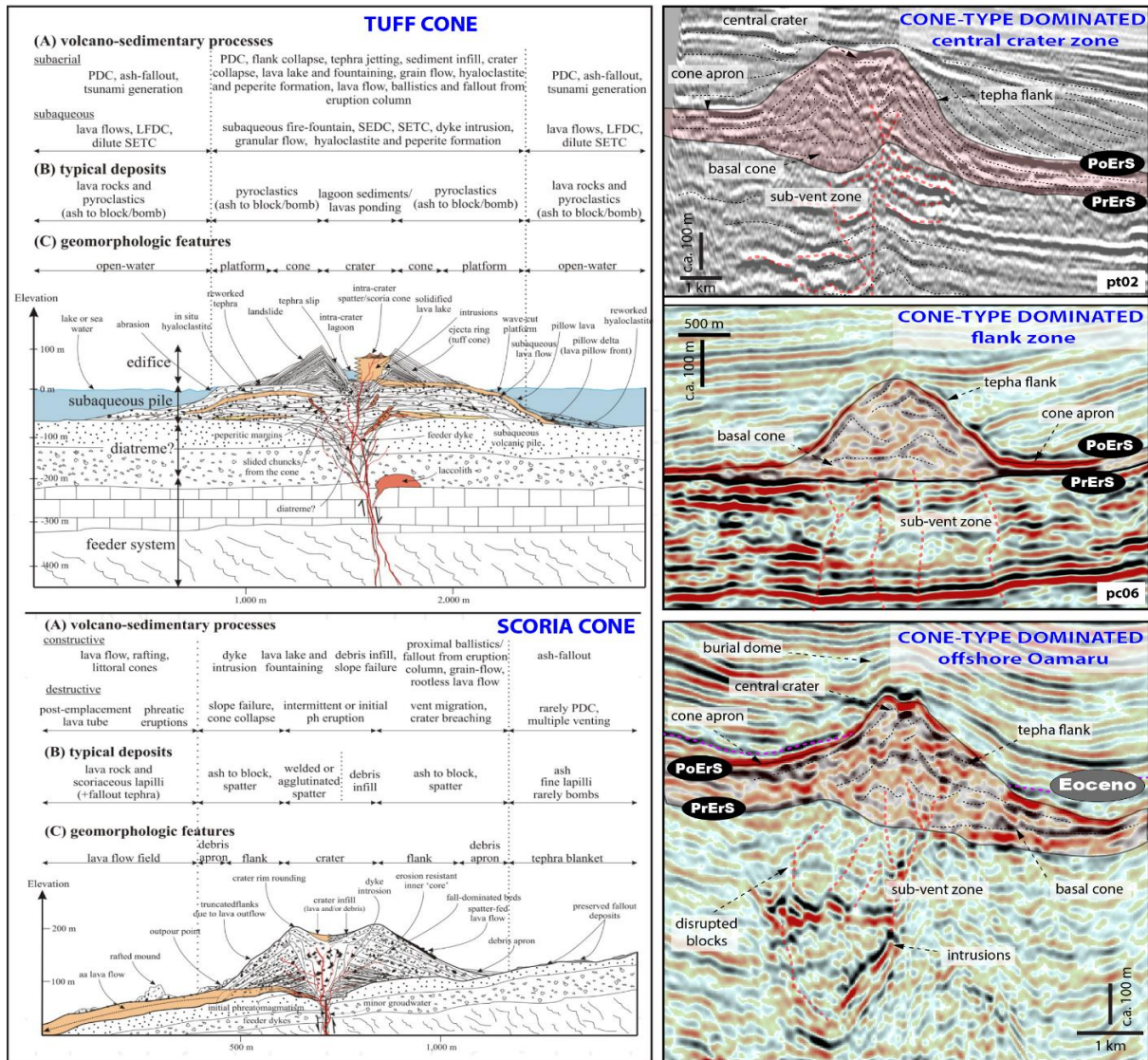
Figure 15: Images on the left-hand side show schematic cross-sections through tuff and scoria cones showing their typical volcano-sedimentary processes, deposits and morphology (from Kereszturi and Németh, 2013). Seismic images on the right-hand side show interpreted 2D lines of MVS cone-type volcanoes, and their large-scale architecture. The seismic section in the lower right-hand corner shows a buried submarine Eocene volcano 40 km offshore of Oamaru (Barrier et al., 2017), which we use as analogue for our interpretations.

Figure 16: Uninterpreted (left) and interpreted (right) 2D seismic line showing the main architectural elements related to cone-type in the MVS. Numbers in red circles are syn-intrusive architectural elements, in green syn-eruptive, and in yellow post-magmatic architectural elements. We observe that cone-type volcanoes are mainly composed of a basal cone, a central crater, a tephra flank and a cone apron. These volcano-types produce upward convex morphologies between the PrErS and PoErS horizons, which we have interpreted to represent the submarine equivalents of tuff cones. Note that the central-crater show inward dipping reflectors while the tephra flank shows outward-dipping reflectors and minor excavation into the PrErS horizon.
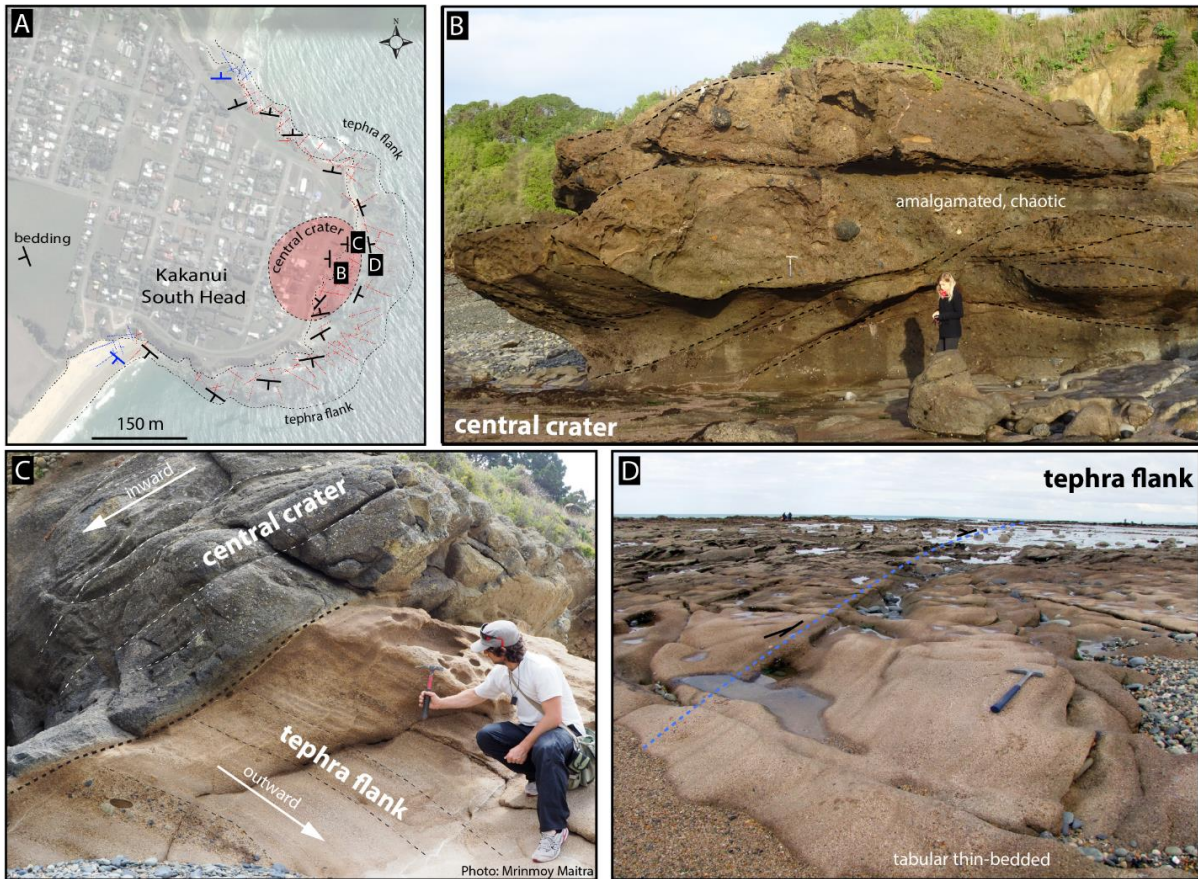
Figure 17: Photographs of potential analogue for MVS syn-eruptive architectural elements outcropping in Kakanui South Head submarine volcanic edifice, near Oamaru, South Island of New Zealand. A) Map showing the location of the vent and flanks of the cone. B) Massive, chaotic, to amalgamated intra-crater lapilli-tuff to tuff-breccia interpreted to be deposited by tephra jets, ballistic and debris flow of material remobilized into the central crater (Corcoran and Moore, 2009; Moorhouse; 2015). C) Angular contact between amalgamated beds inward dipping towards the central crater, and tabular layers of tephra outward-dipping towards the flanks of the edifice. D) Thin-bedded, tabular, semi-circular layers of lapilli-tuff formed by low-volume tephra jetting and eruption-fed density currents deposited at the flanks of the volcanic edifice (Corcoran and Moore, 2009; Kaulfuss et al., 2012).
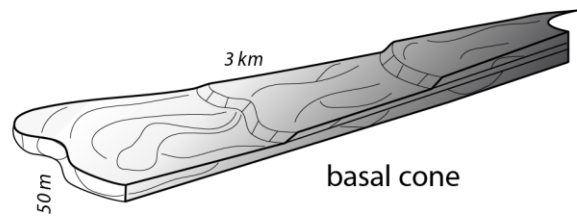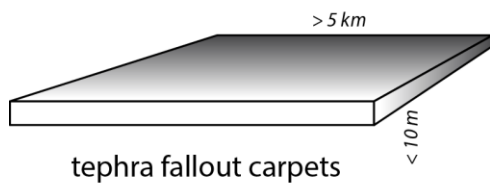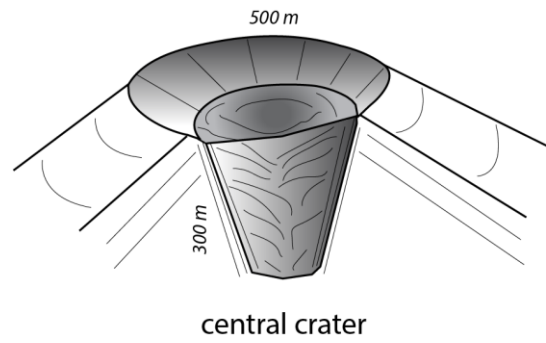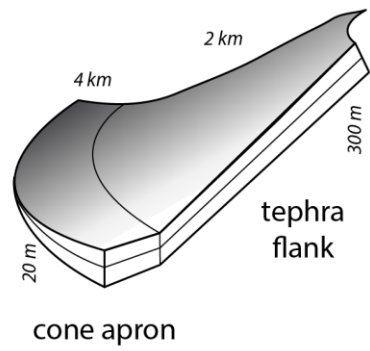
Figure 18: Three-dimensional representation of the main syn-eruptive architectural elements of cone-type volcanoes of the MFV and their average size. Each of these large scale elements can contain sets of smaller-scale architectural elements formed by the interplay of volcanism and concomitant sedimentation.
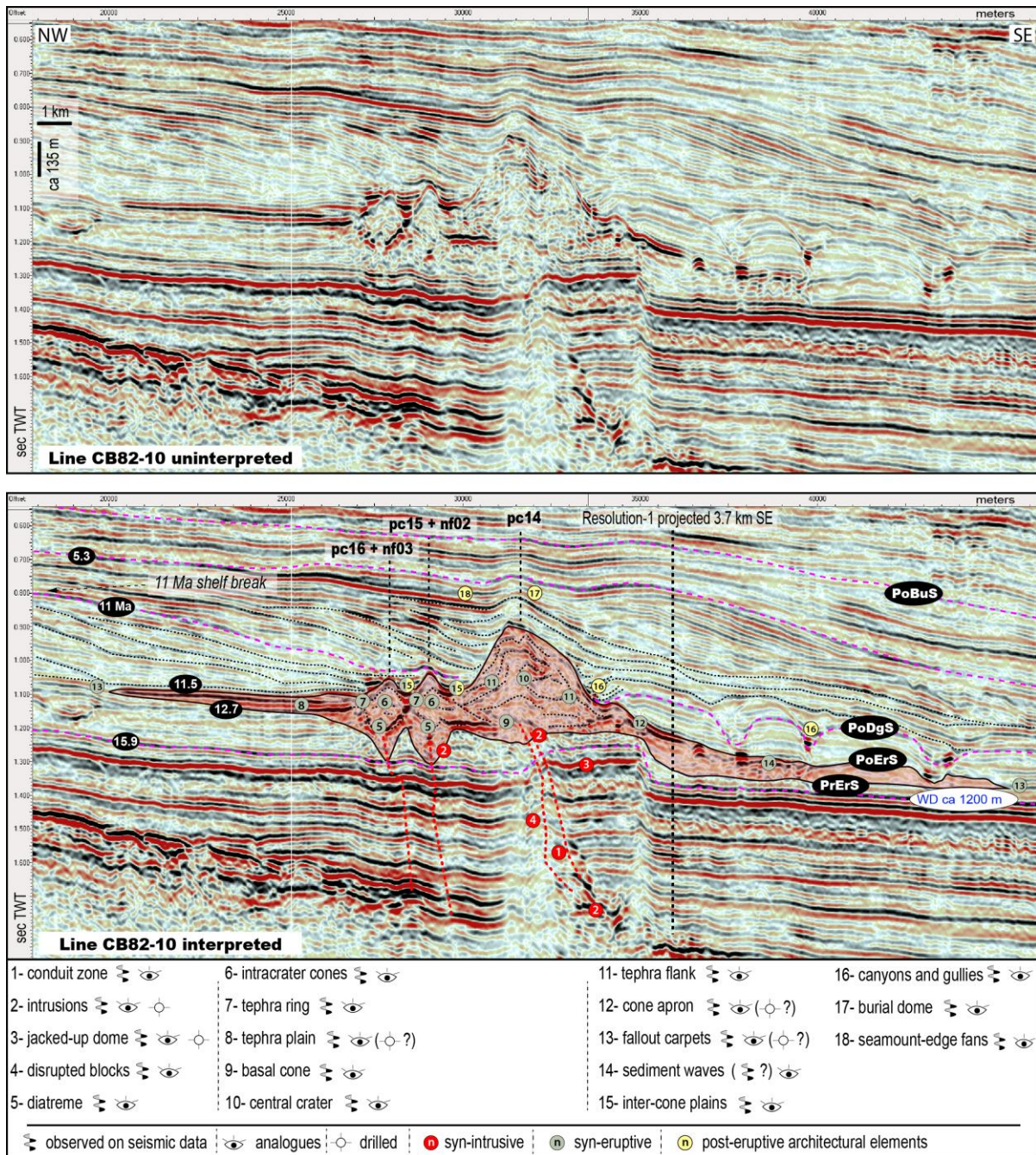
Figure 19: Uninterpreted (above) and interpreted (below) 2D seismic line showing the main architectural elements related to cone-type volcanoes in the MVS. Numbers highlighted in red are syn-intrusive architectural elements, in green syn-eruptive, and in yellow post-magmatic architectural elements. Based on seismic stratigraphic interpretation, the lower sequence of volcanoclastics recovered in Resolution-1 was probably sourced from volcanoes located towards NW or W of the well (likely nf02 and nf03). Tuffs from -1103 to -1110 m depth were likely vented from pc14. WD is the estimated water depth at the time of the formation of these volcanos.
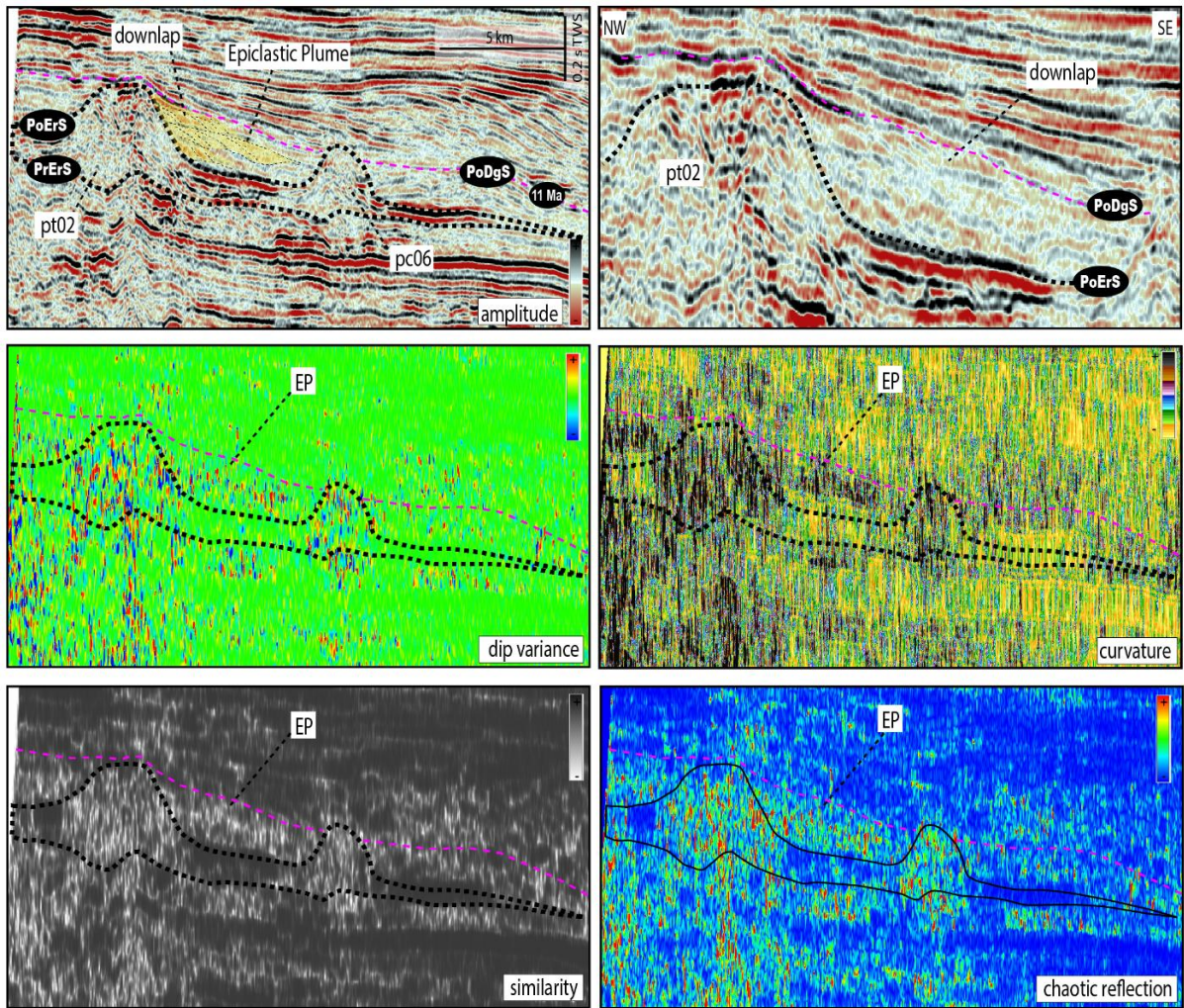
Figure 20: Seismic attribute analysis of pt02 and pc06 volcanoes. Note that the seismic attributes show similarity between the internal and external parts of pt02, which we interpreted as a plume of sediments deposited after erosion of extinct volcanic islands during the degradational stage.
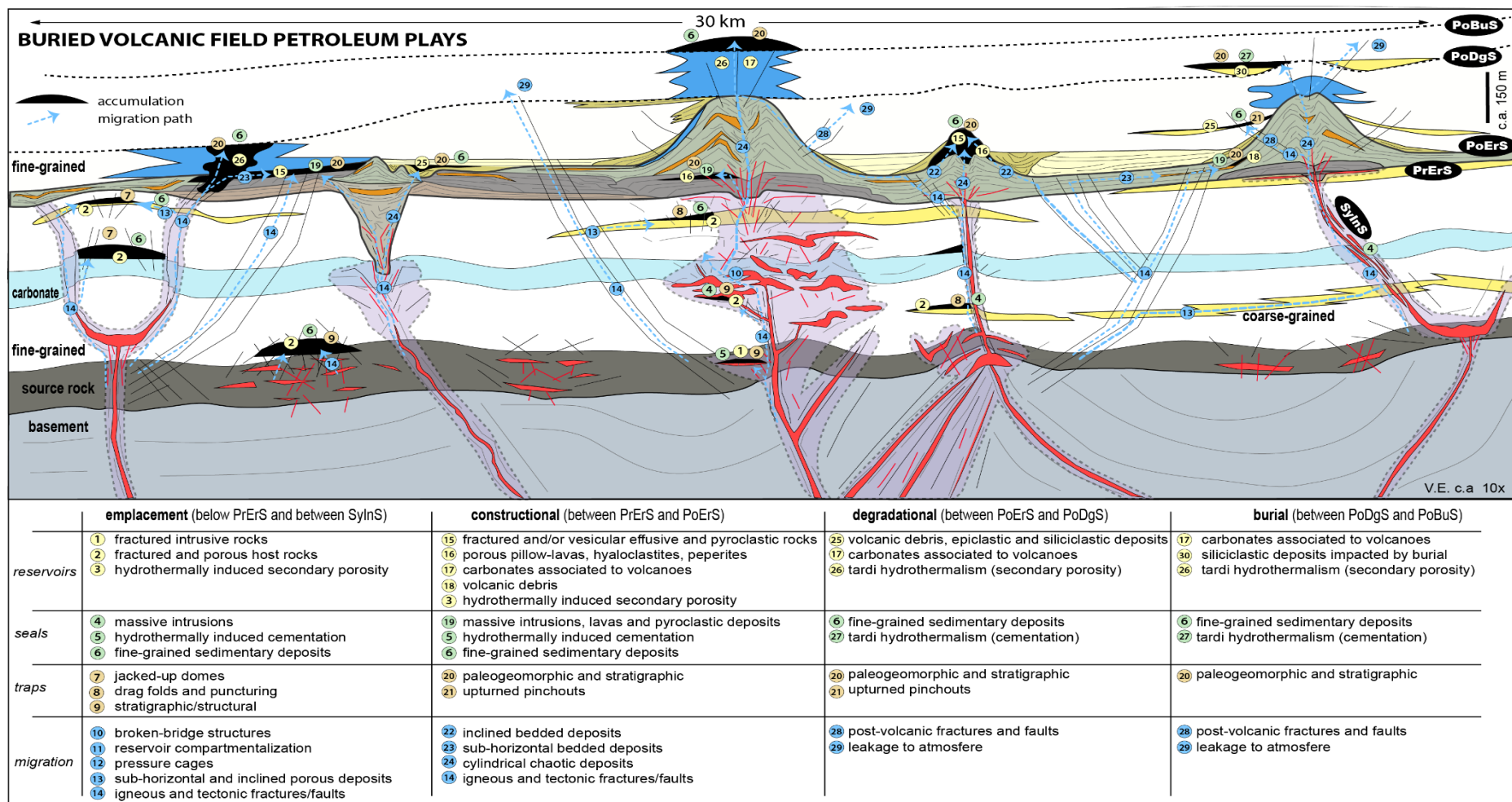
.

Figure 21: Schematic representation of the possible petroleum plays associated with buried monogenetic volcanic systems, based on the observation of the MVS architectural elements. Distinctive sets of architectural elements can create prospective plays according to the magmatic stages of emplacement, construction, degradation, and burial of the volcanoes. Sandstones below the PrErS (yellow), limestones above the PoErS (blue) and faults were added to this model to illustrate possible plays formed by the interaction of these lithologies with volcanic activity.
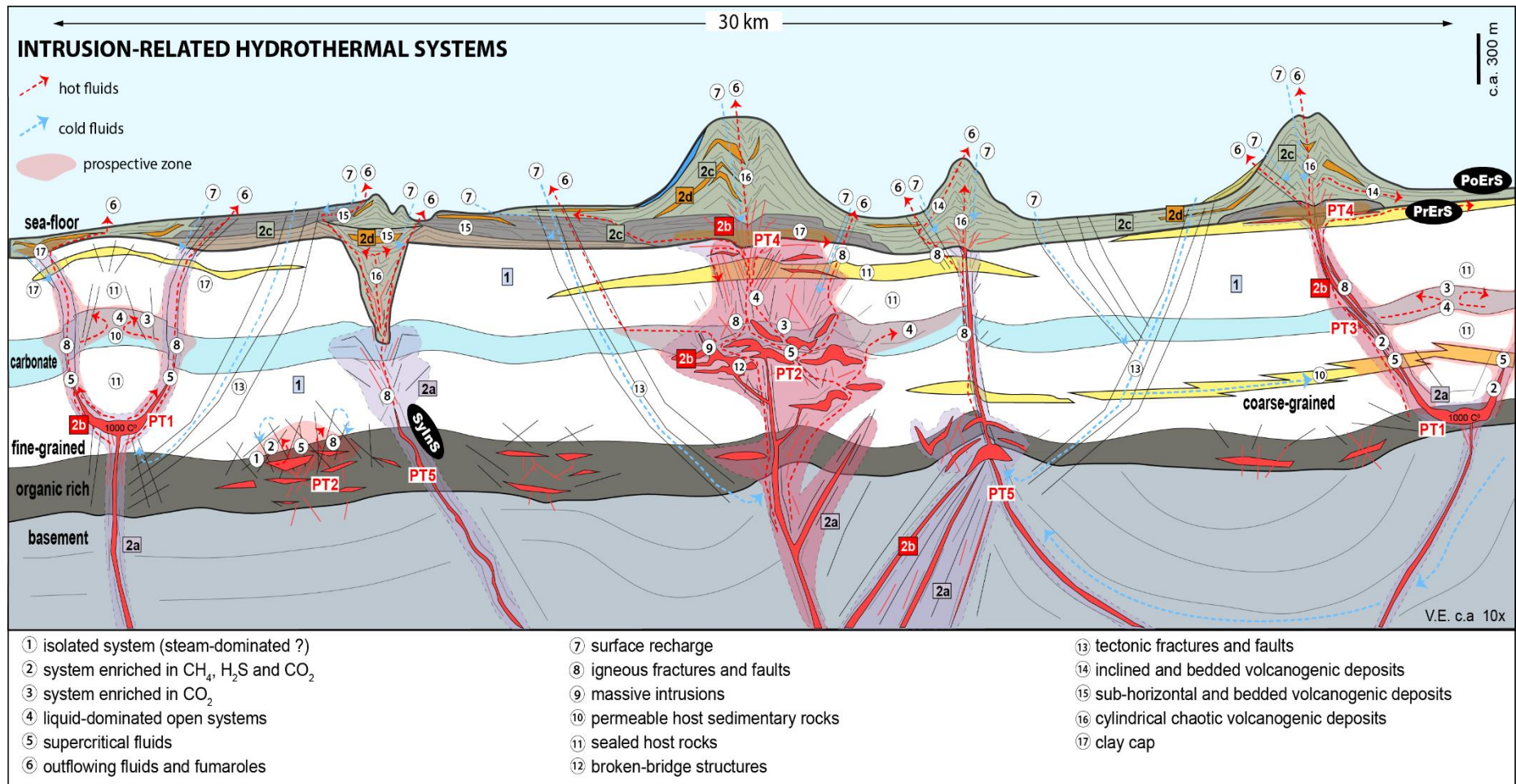
Figure 22: Schematic representation of the possible intrusion-related hydrothermal systems associated with buried monogenetic volcanic systems, based on the observation of MVS architectural elements. Distinctive sets of intrusive architectural elements can create prospective geothermal plays according to their plumbing-types and interactions with diverse types of host rocks.

Table 1: Main characteristics of the stratigraphic surfaces that bound distinctive magmatic sequences and stages in the MVS.

Stratigraphic Surface	Abbr.	Contact relationship	Defined by	Time-relative	Typical architectural elements associated
Post-burial surface	PoBuS	Conformable to both degradational and constructional stages.	Arbitrary surface that limits the relative influence of MVS basin architecture.	Can be synchronous or strongly diachronous (> 5 Ma) from diverse eruptive centres.	Top of the burial dome and associated seamount-edge fans.
Post-degradational surface	PoDgS	Erosional into constructional stage. Laterally conformable within burial stage.	Arbitrary surface relative to one or more eruption centres, for which the rate of burial exceeds the rate of degradation.	Can be synchronous or diachronous from diverse eruptive centres. (> 1 Ma and < 2 Ma)	Epiclastic debris deposits proximal to volcanic edifices and distal non-volcanogenic sedimentary deposits. Canyons and gullies, inter-cone plains.
Post-eruptive surface	PoErS	Overlies the constructional stage. Amalgamated or parallel with the PrErS for increasing distance from eruptive centres.	Younger (in age) eruptive event in MVS.	Minor diachronous from diverse eruptive centres. (Usually < 1 Ma. Max 1.5 Ma)	Epiclastic debris deposits proximal to volcanic edifices and distal non-volcanogenic sedimentary deposits that overlay PoErS.
Pre-eruptive surface	PrErS	Overlies the pre-magmatic sequence and the emplacement stage.	Older (in age) eruptive event in MVS.	Minor diachronous from diverse eruptive centres. (Usually < 1 Ma. Max 1.5 Ma)	Primary eruptive and eruption-related deposits that overlay PrErS.
Syn-intrusive surface	SyInS	Cross-cut the pre-magmatic sequence. Eventual minor cross-cutting into the constructional stage near eruptive centres or at very shallow intrusions.	Presence of intrusive bodies and strata deformed by magmatism.	Minor diachronous from diverse eruptive centres. (Usually < 1 Ma. Max 1.5 Ma)	Dikes, sills, laccoliths, stocks, saucer-shaped sills, and disrupted blocks.

Table 2: Main characteristics of the syn-intrusive architectural elements in the MVS.

Element	Association	Seismic facies	Bounding surfaces	Geometry	Indicative process
Sills	Plumbing-types 2 and 4.	Anomalous single, high amplitude semi-continuous horizontal reflector.	Sharp contact between single high amplitude reflector and external bedded seismic facies.	Tabular horizontal to sub-horizontal.	Rock body emplaced parallel within enclosing strata.
Saucer-shaped sills	Plumbing-type 1 and 2.	Typically single high amplitude, semi-	Sharp contact between single high amplitude reflector	Saucer-like.	Rock body emplaced parallel within enclosing strata. Jack-up, brittle deformation

		continuous, horizontal to inclined reflector.	and external bedded seismic facies.		and body cross-cutting enclosing strata.
Dikes	Plumbing-types 3, 4 and 5.	Single, narrow, vertical to sub-vertical transparent (i.e. reflector-free) discontinuities in bedded strata.	Sharp contact between sub-vertical transparent discontinuities and external bedded seismic facies.	Tabular vertical to sub-vertical. Typically seismically unresolved.	Rock body cross-cutting enclosing strata.
Dikes-and- sills swarm	Plumbing-types 2, 3 and 4.	Multiple high amplitude, discontinuous, horizontal to steeply inclined reflectors in chaotic configuration.	Sharp contacts between multiple, chaotic, high amplitude reflectors and external bedded seismic facies.	Complex, chaotic.	Multiple rock bodies cross-cutting and parallel emplacing within bedded strata.
Stocks and laccoliths	Plumbing-types 2 and 3.	Single, thick, high amplitude, typically continuous, semi-circular reflector.	Sharp contacts between high amplitude reflectors and external seismic facies.	Sub-geoidal. Not always resolved in seismic data.	Rock body cross-cutting enclosing strata.
Disrupted blocks	Plumbing-types 1, 2, 3, 4 and 5.	Multiple narrow, vertical to sub-vertical transparent discontinuities in bedded strata.	Sharp contact between sub-vertical transparent discontinuities and external bedded seismic facies.	Chaotic.	Brittle deformation of bedded strata.
Jacked-up domes	Plumbing-types 1, 2, and 3.	Bedded strata domed above typically single high amplitude, semi-continuous, horizontal to inclined reflector.	Gradational contact between domed and parallel bedded seismic facies.	Downward-concave dome.	Strata jacked up above rock body emplaced parallel within enclosing strata.

Table 3: Main characteristics of the architectural elements of the crater-type dominate volcanoes formed during the constructional magmatic stage in the MVS.

Element	Location	Seismic facies	Bounding surfaces	Geometry	Indicative processes
Root zone	Bottom of the funnel-like structure.	Moderate to high amplitude and disrupted reflectors showing depression towards the centre of the structure.	Seismically unresolved.	Unsure, probably geoidal.	Brittle deformation. Post-eruptive subsidence?
Lower diatreme	Centre of the funnel-like structure.	Moderate amplitude, discontinuous and chaotic reflectors.	Sharp contact between internal unbedded seismic facies from external bedded reflectors.	Funnel-like.	Brittle deformation. Excavation into PrErS. Intense fragmentation and dispersion of material.
Upper diatreme	Top of the funnel-like structure.	Moderate amplitude, semi-continuous, parallel and sub-	Sharp contact between Internal bedded seismic facies from external unbedded seismic	Funnel-like.	Deposition of layered material into an upper crater.

Element	Location	Seismic facies	Bounding surfaces	Geometry	Indicative processes
		horizontal reflectors.	facies below, and mound-like facies above.		
Tephra ring	Symmetrically lateral to the upper diatreme.	Single high amplitude, continuous and inclined reflectors in A shape.	Sharp contacts between the upper and lower limits of the high amplitude reflector. Laterally gradational to facies of the ring plain.	Ring-like.	Deposition of "hard" material in relatively steep repose angle near a vent zone.
Ring plain	Symmetrically lateral to the tephra ring.	Single high amplitude, continuous, parallel and sub-horizontal reflectors.	Sharp contacts between upper and lower limits of the high amplitude reflector. Laterally gradational to facies of the ring plain. Fade with increasing distance from the vent zone.	Circular tabular, thinner with increasing distance from the vent.	Intense fragmentation and dispersion of material ejected from the diatreme. Deposit parallel to basin sediments immediately above PrErS.
Intra-crater cones	Above of the funnel-like structure.	Moderate amplitude reflector with mound-like shape and transparent internal seismic facies.	Sharp contacts between the upper and lower limits of the mound-like structure and external bedded facies.	Mound-like and possible small cone-like.	Deposition of material above the upper diatreme. Late eruptive events?
Overspill wedge	Symmetrically lateral to the intra-crater cones.	High-to-low amplitude, discontinuous reflectors that together show a wedge shape.	Sharp contacts between upper and lower limits of the wedge-like structure. Fade with increasing distance from the vent zone.	Circular wedge-like.	Material that overspill the tephra ring and deposit parallel to basinal sediments immediately above the ring plain.
Tephra fallout carpet	Seismically unresolved, but probably distal to the funnel-like structure.	Seismically unresolved, but probably amalgamated with reflectors that represent basinal sediments.	Seismically unresolved, but probably sharp and parallel contact between volcanoclastics and Tokama Siltstone (wire-logs of the Resolution-1)	Seismically unresolved, but probably tabular.	Probably represent thin and tabular layers of tephra interbedded with basinal sediments.

Table 4: Main characteristics of the architectural elements of the cone-type dominate volcanoes formed during the constructional magmatic stage in the MVS.

Element	Location	Seismic facies	Bounding surfaces	Geometry	Indicative processes
Basal cone	Bottom of the cone-like structure.	Moderate to high amplitude sub-horizontal and parallel reflectors.	Sharp to gradational contact between internal sub-horizontal and parallel facies, from external seismic facies	Unsure, probably tabular.	Material piled-up near vent, sub-parallel to basin sediments

			with inclined, disrupted or chaotic reflectors		and above the PrErS.
Central crater or vent zone	Centre of the cone-like structure.	Typically transparent, but also show moderate to low amplitude, discontinuous, chaotic or parallel reflectors dipping inward the central crater.	Sharp to erosive contact between internal chaotic seismic facies from external facies typically bedded and inclined.	Probably cylindrical based in analogues.	Material disperse out of the crater zone. Chaotic deposits probably represent collapses of the crater walls, and deposition of intra-crater layers of tephra.
Tephra flank	Symmetrically lateral to the central crater.	Moderate to low amplitude, semi-continuous, parallel and inclined reflectors dipping outwards from the central crater zone.	Sharp to erosive contact between internal inclined and bedded seismic facies from external chaotic (towards the central crater) or sub-parallel seismic facies (towards the basin).	Conical.	Deposition of layered material near a vent zone and above the basal cone, or above PrErS.
Cone apron	Symmetrically lateral to the tephra flank.	Low to high amplitude, typically continuous and sub-parallel and sub-horizontal reflectors.	Sharp to gradational between bedded seismic facies that pinch with increasing distance from the eruptive centre.	Ring-like.	Deposition of material distal to a vent zone and above PrErS
Tephra fallout carpet	Seismically unresolved, but probably distal to the funnel-like structure.	Seismically unresolved, but probably amalgamated with reflectors that represent basin sediments.	Seismically unresolved, but probably sharp and parallel contact between volcanoclastics and Tokama Siltstone (wire-logs of the Resolution-1)	Seismically unresolved, but probably tabular.	Probably represent thin and tabular layers of tephra interbedded with basin sediments.

1.1 References

Aarnes, I., Planke, S., Trulsvik, M., Svensen, H., 2015. Contact metamorphism and thermogenic gas generation in the Vøring and Møre basins, offshore Norway, during the Paleocene-Eocene thermal maximum. Journal of the Geological Society, 172(5), 588-598.

Agirrezabala, L., Sarrionandia, F., Carracedo, M., 2017, Diatreme-forming volcanism in a deep-water faulted basin margin: Lower Cretaceous outcrops from the Basque-Cantabrian Basin, western Pyrenees. Journal of Volcanology and Geothermal Research. https://doi.org/10.1016/j.jvolgeores.2017.03.019

Allen, J. R. L., 1983, Studies in Fluviatile Sedimentation: Bars, Bar-Complexes and Sandstone Sheets (Low-Sinuosity Braided Streams) in the Brownstones (L.

Devonian), Welsh Borders: Sedimentary Geology, 33 (4): 237–93. doi:10.1016/0037-0738(83)90076-3.

Arnórsson, S., S. Thórhallsson., A. Stefánsson., 2015, Utilization of Geothermal Resources, in The Encyclopedia of Volcanoes: https://doi.org/10.1016/B978-0-12-385938-9.00071-7

Barata, C. F., M. V. Caputo,. 2007. Geologia Do Petróleo Da Bacia Do Solimões. O "Estado Da Arte". In 4o Pdpetro.

Barrier, A., A. Nicol, A. P. Bischoff., 2017, Volcanism Occurrences in the Canterbury Basin, New Zealand and Implication for Petroleum Exploration. In AAPG GTW Influence of Volcanism and Associated Magmatic Processes on Petroleum Systems. Conference, Oamaru New Zealand.

Barrier, submitted. Tectonic, structure and sedimentary evolution of the Canterbury Basin, New Zealand. PhD Thesis, University of Canterbury.

Bergman, S.C., J.P. Talbot, and P.R. Thompson., 1992, The Kora Miocene Submarine Andesite Stratovolcano Hydrocarbon Reservoir, Northern Taranaki Basin, New Zealand. In 1991 New Zealand Oil Exploration Conference, 178–206.

Bischoff, A.P., A. Nicol, A. Barrier, M. Beggs., 2016, The Stratigraphic Record of Volcanism - Examples from New Zealand Sedimentary Basins. In 2016 Geoscience Society of New Zealand Conference, Wanaka, Abstract.

Bischoff, A. P., A. Nicol, M. Beggs., 2017, Stratigraphy of architectural elements in a buried volcanic system and implications for hydrocarbon exploration: Interpretation, https://doi.org/10.1190/INT-2016-0201.1

Bischoff, A.P., A. Barrier., A. Nicol., W. Mohriak., 2018, Carbonate Build-up on Volcanic Highs - Global Petroleum Plays and Analogues from New Zealand Sedimentary Basins. In 2018 Brazilian Petroleum Conference, Rio de Janeiro, Brazil, Abstract.

Bischoff, A.P., 2019, Architectural Elements of Buried Volcanic Systems and Their Impact on Geoenergy Resources. Ph.D. Thesis, Canterbury University, New Zealand. Pre-print, 226p. doi: 10.13140/RG.2.2.21440.58886

Blanke, S. J., 2012, "Saucer Sills" of the Offshore Canterbury Basin: GNS Publication, https://doi.org:10.1177/0094306114545742f

Bonadonna, C., G. C. Mayberry, E. S. Calder, R. S. J. Sparks, C. Choux, P. Jackson, A. M. Lejeune, S. C. Loughlin, G. E. Norton, W. I. Rose, G. Ryan, S. R. Young., 2002, Tephra fallout in the eruption of Soufrière Hills Volcano, Montserrat: Geological Society, London, Memoirs, doi:10.1144/GSL.MEM.2002.021.01.22.

Borghi, L., 2000, Visão geral da análise de fácies do ponto de vista da arquitetura deposicional. Boletim do Museu Nacional. Nova Série Geologia, Rio de Janeiro, v. 53, n.58, p. 1-26.

Carlotto, M. A., R. C. B. Silva., A. A. Yamato., W. L. Trindade., J. L. P. Moreira., R. A. R. Fernandes, O. J. S. Ribeiro., et al. 2017. Libra: A Newborn Giant in the Brazilian Presalt Province. In Gialnt Fields of the Decade 2000-2010. doi:10.1306/13572006M1133685

Cas, R. A. F., Landis, C. A., and Fordyce, R. E., 1989, A monogenetic, Surtla-type, Surtseyan volcano from the Eocene-Oligocene Waiareka-Deborah volcanics, Otago, New Zealand: A model: Bulletin of Volcanology, v. 51, no. 4, p. 281-298.

Cas, R. A. F., J. V. Wright., 1993, Volcanic Successions: Modern and Ancient - A Geological Approach to Processes, Products and Successions. Chapman and Hall, UK. https://doi.org:10.1007/978-0-412-44640-5

Cas, R. A. F., G. Giordano., 2014, Submarine volcanism: A review of the constraints, processes and products, and relevance to the Cabo de Gata volcanic succession: https://doi.org:10.3301/IJG.2014.46

Cas, R. A. F., J. M. Simmons., 2018, Why Deep-Water Eruptions Are So Different From Subaerial Eruptions: Frontiers in Earth Science, v. 6, p. 198, doi:10.3389/feart.2018.00198

Catuneanu, O., 2006, Principles of Sequence Stratigraphy. Changes, 375. https://doi.org:10.5860/CHOICE.44-4462

Catuneanu, O., Abreu, V., Bhattacharya, J.P., Blum, M.D., Dalrymple, R.W., Eriksson, P.G.,Fielding, C.R., Fisher, W.L., Galloway, W.E., Gibling, M.R., Giles, K.A., Holbrook, J.M.,Jordan, R., Kendall, C.G.St.C., Macurda, B., Martinsen, O.J., Miall, A.D., Neal, J.E.,Nummedal, D., Pomar, L., Posamentier, H.W., Pratt, B.R., Sarg, J.F., Shanley, K.W.,Steel, R.J., Strasser, A., Tucker, M.E., Winker, C., 2009, Towards the standardization of sequence stratigraphy. Earth-Science Reviews 92, 1–33. Elsevier B.V.: 1–33. doi:10.1016/j.earscirev.2008.10.003

Catuneanu, O., W. E. Galloway, C.G. St. C. Kendall, A. D. Miall, H. W. Posamentier, A. Strasser., M. E. Tucker., 2011, Sequence Stratigraphy: Methodology and Nomenclature. Newsletters on Stratigraphy. doi:10.1127/0078-0421/2011/0011

Catuneanu, O., J. P. Bhattacharya, M. D. Blum, R. W. Dalrymple, P. G. Eriksson, C. R. Fielding, W. L. Fisher, et al., 2010, Sequence Stratigraphy: Common Ground after Three Decades of Development. First Break. doi:10.3997/1365-2397.2010002

Chadwick, W. W., R. P. Dziak, J. H. Haxel, R. W. Embley, H. Matsumoto., 2012, Submarine landslide triggered by volcanic eruption recorded by in situ hydrophone: Geology, v. 40, no. 1, p. 51–54, doi:10.1130/G32495.1

Chorowicz, J., 2005, The East African rift system: Journal of African Earth Sciences, v. 43, no. 1, p. 379–410, doi:https://doi.org/10.1016/j.jafrearsci.2005.07.019.

Clague, D., R. Batiza., J.W. Head., A. Davis.,2000a, Pyroclastic and Hydroclastic Deposits on Loihi Seamount, Hawaii, in Explosive Subaqueous Volcanism, edited by J.D.L. White, J.L. Smellie, and D.A. Clague, American Geophysical Union, Washington D.C., 200. Bulletin of Volcanology. https://doi.org/10.1029/140GM05

Coombs, D. S., A. J. R. White., D. Hamilton., and R. A. Couper., 1960, Age relations of the Dunedin volcanic complex and some paleogeographic implications—Part II: New Zealand Journal of Geology and Geophysics, https://doi.org:10.1080/00288306.1960.10420145

Coombs, D.S., Cas, R.A., Kawachi, Y., Landis, C.A., McDonough, W.F., Reay, A., 1986, Cenozoic volcanism in north, east and central Otago. In: Smith, I.E.M. (Ed.), Late Cenozoic Volcanism in New Zealand. R. Soc. N.Z. Bull. 23, pp. 278-312.

Corcoran, P. L., L. N. Moore., 2008, Subaqueous eruption and shallow-water reworking of a small-volume Surtseyan edifice at Kakanui, New Zealand: Canadian Journal of Earth Sciences, v. 45, no. 12, p. 1469-1485.

Deardorff, N. D., K. V. Cashman., W. W. Chadwick., 2011, Observations of eruptive plume dynamics and pyroclastic deposits from submarine explosive eruptions at NW Rota-1, Mariana arc: Journal of Volcanology and Geothermal Research, https://doi.org/10.1016/j.jvolgeores.2011.01.003

Deegan, F. M., V. R. Troll., C. Freda., V. Misiti., J. P. Chadwick., C. L. McLeod., J. P. Davidson., 2010, Magma–Carbonate Interaction Processes and Associated CO_2 Release at Merapi Volcano, Indonesia: Insights from Experimental Petrology. Journal of Petrology 51 (5): 1027–51. doi.org/10.1093/petrology/egq010

Delmelle, P., E. Maters., C. Oppenheimer., 2015, Volcanic Influences on the Carbon, Sulfur, and Halogen Biogeochemical Cycles, in The Encyclopedia of Volcanoes: doi:10.1016/B978-0-12-385938-9.00050-X

Di Capua, A., G. Groppelli., 2016, Emplacement of pyroclastic density currents (PDCs) in a deep-sea environment: The Val d'Aveto Formation case (Northern Apennines, Italy): Journal of Volcanology and Geothermal Research, doi:10.1016/j.jvolgeores.2016.08.003

Field, B.D., Browne, G.H., Davy, B.W., Herzer, R.H., Hoskins, R.H., Raine, J.I., Wilson, G.J., Sewell, R.J., Smale, D., Watters, W.A., 1989 Cretaceous and Cenozoic sedimentary basins and geological evolution of the Canterbury region, South Island, New Zealand. Lower Hutt: New Zealand Geological Survey. New Zealand Geological Survey basin studies 2. 94 p.

Finn, C. A., R. D. Müller., K. S. Panter., 2005, A Cenozoic diffuse alkaline magmatic province (DAMP) in the southwest Pacific without rift or plume origin: Geochemistry, Geophysics, Geosystems, https://doi.org/10.1029/2004GC000723

Fiske, R.S., Cashman, K.V., Shibata, A., Watanabe, K., 1998, Tephra dispersal from Myojinsho, Japan, during its shallow submarine eruption of 1952–1953: Bulletin of Volcanology , v. 59, p. 262–275, doi:10.1007/s004450050190.

Galland, O., Bertelsen, H.S., Eide, C.H., Guldstrand, F., Haug, Ø.T., Héctor, Leanza, A., Mair, K., Palma, O., Planke, S., Rabbel, O., Rogers, B., Schmiedel, T., Souche, A., Spacapan, J.B., 2018, Storage and transport of magma in the layered crust-Formation of sills and related float-lying intrusions, in Volcanic and Igneous Plumbing Systems, edited by S. Burchardt, pp. 111-136, Elsevier.

Gamboa, D., T. M. Alves., 2015, Spatial and Dimensional Relationships of Submarine Slope Architectural Elements: A Seismic-Scale Analysis from the Espírito Santo Basin (SE Brazil). Marine and Petroleum Geology. doi:10.1016/j.marpetgeo.2015.02.035.

Goff, F., Janik, C.J., 2000, Geothermal Systems, Encyclopedia of Volcanoes, Academic Press, Chapter-49, pp. 817 – 834.

Grove, T. L., C. B. Till, 2015, Melting the Earth's Upper Mantle, in The Encyclopedia of Volcanoes: doi:10.1016/B978-0-12-385938-9.00001-8.

Hansen, D. M., J. Cartwright., 2006, Saucer-Shaped Sill with Lobate Morphology Revealed by 3D Seismic Data: Implications for Resolving a Shallow-Level Sill Emplacement Mechanism. Journal of the Geological Society 163 (3): 509–23. https://doi.org/10.1144/0016-764905-073

Hansen, D.M., 2006. The morphology of intrusion-related vent structures and their implications for constraining the timing of intrusive events along the NE Atlantic Margin. J. Geol. Soc. 163, 789–800.

Heap, M. J., B. M. Kennedy., 2016, Exploring the scale-dependent permeability of fractured andesite: Earth and Planetary Science Letters, doi:10.1016/j.epsl.2016.05.004.

Heap, M. J., B. M. Kennedy., J. I. Farquharson., J. Ashworth., K. Mayer., M. Letham-Brake., T. Reuschlé., H. A. Gilg., B. Scheu., Y. Lavallée., P. Siratovich., J. Cole., A. D.

Jolly., P. Baud., D. B. Dingwell., 2017, A multidisciplinary approach to quantify the permeability of the Whakaari/White Island volcanic hydrothermal system (Taupo Volcanic Zone, New Zealand): Journal of Volcanology and Geothermal Research, doi:10.1016/j.jvolgeores.2016.12.004

Herzer, R. H., Seismic Stratigraphy of a Buried Volcanic Arc, Northland, New Zealand and Implications for Neogene Subduction. Marine and Petroleum Geology 12, no. 5 (January 1995): 511–31. https://doi.org/10.1016/0264-8172(95)91506-K

Holford, S. P., N. Schofield, J. D. MacDonald, I. R. Duddy, P. F. Green., 2012, Seismic Analysis of Igneous Systems in Sedimentary Basins and Their Impacts on Hydrocarbon Prospectivity: Examples from the Southern Australian Margin. APPEA Journal, 52, 229–52.

Holford, S., N. Schofield, and P. Reynolds., 2017, Subsurface fluid flow focused by buried volcanoes in sedimentary basins: Evidence from 3D seismic data, Bass Basin, offshore southeastern Australia: 39-50 p., doi:10.1190/INT-2016-0205.1.

Iacono-Marziano, G., Morizet, Y., Le Trong, E., Gaillard, F., 2013, New experimental data and semi-empirical parameterization of H_2O-CO_2 solubility in mafic melts. Geochimica Et Cosmochimica Acta 97. 145-157.

Infante-Paez, L., and K. J. Marfurt, 2017, Seismic expression and geomorphology of igneous bodies: A Taranaki Basin, New Zealand, case study: Interpretation, v. 5, no. 3, p. SK121-SK140, https://doi.org/10.1190/INT-2016-0244.1

Iyer, K., Rupke, L., Galerne, C.Y., 2013. Modeling fluid flow in sedimentary basins with sill intrusions: Implications for hydrothermal venting and climate change. Geochem. Geophys. Geosyst. 14, 5244–5262.

Jackson, C. A.-L., 2012, Seismic reflection imaging and controls on the preservation of ancient sill-fed magmatic vents: Journal of the Geological Society, https://doi.org/10.1144/0016-76492011-147

Jamtveit, B., Svensen, H., Podladchikov, J.J., Planke, S., 2004. Hydrothermal vent complexes associated with sill intrusions in sedimentary basins. Geol. Soc. Lond., Spec. Publ. 234, 233-241.

Jerram, D. A., R. T. Single., R. W. Hobbs., C. E. Nelson., 2009, Understanding the offshore flood basalt sequence using onshore volcanic facies analogues: An example from the Faroe-Shetland basin: Geological Magazine, https://doi.org/10.1017/S0016756809005974

Jiachao, H., 2012. Assessment and Management of Sedimentary Geothermal Resources.Master Thesis. Faculty of Earth Sciences University of Iceland.

Jones, A., D., G. Wilson., A. Gorman., B. Fox., D. Lee., U. Kaulfuss., 2017, A drill-hole calibrated geophysical characterisation of the 23 Ma Foulden Maar stratigraphic sequence, Otago, New Zealand: 1-13 p., https://doi.org/10.1080/00288306.2017.1369130

Kaulfuss, U., K. Németh, and J. White., 2012, Field Guide Miocene subaerial to subaqueous monogenetic volcanism in Otago, New Zealand.

Kendall, C. G. C., Tucker, M. E., 2010, SEPM STRATA website. http://www.sepmstrata.org/page.aspx?pageid=410

Kereszturi, G., G. Csillag., K. Németh., K. Sebe., K. Balogh., and V. Jáger., 2010, Volcanic architecture, eruption mechanism and landform evolution of a Plio/Pleistocene intracontinental basaltic polycyclic monogenetic volcano from the Bakony-Balaton Highland Volcanic Field, Hungary: Central European Journal of Geosciences, doi:10.2478/v10085-010-0019-2

Kereszturi, G., K. Németh., G. Csillag., K. Balogh., J. Kovács., 2011, The role of external environmental factors in changing eruption styles of monogenetic volcanoes in a Mio/Pleistocene continental volcanic field in western Hungary: 227-240 p., doi:10.1016/j.jvolgeores.2010.08.018

Kereszturi, G., K. Németh., 2013, Monogenetic Basaltic Volcanoes: Genetic Classification, Growth, Geomorphology and Degradation: Updates in Volcanology - New Advances in Understanding Volcanic Systems, https://doi.org/10.5772/51387

Kiyosugi, K., 2012. Temporal and Spatial Analysis of Monogenetic Volcanic Fields. PhD theses. https://scholarcommons.usf.edu/etd/4101

Lima, B., De Ros, L., 2019, Deposition, diagenetic and hydrothermal processes in the Aptian Pre-Salt lacustrine carbonate reservoirs of the northern Campos Basin, offshore Brazil. Sedimentary Geology. 383. 10.1016/j.sedgeo.2019.01.006

Liu, J. Hou, Y. Li, Y. Dong, X. Ma, X. Wang., 2018, Characterisation of architectural elements of Ordovician fractured-cavernous carbonate reservoirs, Tahe Oilfield, China J. Geol. Soc. India, 91 (3) (2018), pp. 315-322

Lorenz, V., 1985. Maars and diatremes of phreatomagmatic origin, a review. Transactions of the Geological Society of South Africa, 88: 459-470.: 459-470 p.

Lorenz, V. and Kurszlaukis, S., 2007, Root Zone Processes in the Phreatomagmatic Pipe Emplacement Model and Consequences for the Evolution of Maar-Diatreme Volcanoes. Journal of Volcanology and Geothermal Research, 159, 4-32.

Macdonald, R., 2003, Magmatism of the Kenya Rift Valley: A review. Transactions of the Royal Society of Edinburgh: Earth Sciences, 239-253 p., doi:10.1017/S0263593300000420

Magoon, L. B., and W. G. Dow, 1994, The Petroleum System: AAPG Memoir, doi:10.1126/science.51.1323.468.

McLean, C. E., N. Schofield., D. J. Brown., D. W. Jolley., and A. Reid, 2017, 3D seismic imaging of the shallow plumbing system beneath the Ben Nevis Monogenetic Volcanic Field: Faroe–Shetland Basin: Journal of the Geological Society, https://doi.org/10.1144/jgs2016-118

Miall, A. D., 1985, Architectural-Element Analysis: A New Method of Facies Analysis Applied to Fluvial Deposits. Earth-Science Reviews Elsevier Science Publishers B.V 22: 261–308. doi:10.1016/0012-8252(85)90001-7

Miall, A. D., Tyler, N., 1991, Three-Dimensional Facies Architecture of Terrigenous Clastic Sediments and Its Implications for Hydrocarbon Discovery and Recovery. 1–5. SEPM (Society for Sedimentary Geology). doi:10.2110/csp.91.03.0001

Miall, A. D., 2000, Principles of Sedimentary Basin Analysis; Springer-Verlag, New York, 616p.

Millett, J., A. Wilkins., E. Campbell., M. Hole., R. Taylor., D. Healy., D. Jerram., D. Jolley., S. Planke., S. Archer., A. Blischke., 2016, The geology of offshore drilling through basalt sequences: Understanding operational complications to improve efficiency: doi:10.1016/j.marpetgeo.2016.08.010

Milne, A.D., 1975. Well completion report Resolution, for BP, Shell, Todd Canterbury Service Limited. New Zealand Geological Survey Open-file Petroleum Report No. 648.

Mitchum, R M, P. R. Vail., 1977, Seismic Stratigraphy and Global Changes of Sea Level, Part 7 : Seismic Stratigraphic Interpretation Procedure. Seismic Stratigraphy: Applications to Hydrocarbon Exploration. AAPG Memoir 26 Memoir 26: 135–43.

Mohriak, W.U., M. Nemcok., G. Enciso., 2008. South Atlantic divergent margin evolution: rift-border uplift and salt tectonics in the basins of SE Brazil. In: Pankhurst, R.J., Trouw, R.A.J., Brito Neves, B.B. & de Wit, M.J. (eds.), West Gondwana pre-

Cenozoic correlations across the South Atlantic region. Geological Society of London, Special Publication 294, p.365-398.

Montanari, D., M. Bonini,, G. Corti,, A. Agostini,, C. Ventisette., 2017, Forced folding above shallow magma intrusions: Insights on supercritical fluid flow from analogue modelling: doi:10.1016/j.jvolgeores.2017.07.022

Moorhouse, B. L., J. D. L. White, and J. M. Scott, 2015, Cape Wanbrow: A stack of Surtseyan-style volcanoes built over millions of years in the Waiareka-Deborah volcanic field, New Zealand: Journal of Volcanology and Geothermal Research, doi:10.1016/j.jvolgeores.2015.03.019

Moraes, M. A. S., P. R. Blaskovski., P. L. B. Paraizo., 2005, Arquitetura de Reservatórios de Águas Profundas. Boletim de Geociencias Da Petrobras.

Mordensky, S., M. Villeneuve., J. Farquharson., B. Kennedy., M. J. Heap., D. M. Gravley., 2018, Rock mass properties and edifice strength data from Pinnacle Ridge, Mt. Ruapehu, New Zealand: doi:10.1016/j.jvolgeores.2018.09.012

Morley, C., 2018, 3D seismic imaging of the plumbing system of the Kora volcano, Taranaki Basin, New Zealand: The influences of syn-rift structure on shallow igneous intrusion architecture: Geosphere, 2018. doi.org/10.1130/GES01645.1

Muirhead, J. D., A. R. Van Eaton., G. Re, J. D. L. White., and M. H. Ort., 2016, Monogenetic volcanoes fed by interconnected dikes and sills in the Hopi Buttes volcanic field, Navajo Nation, USA: Bulletin of Volcanology, doi:10.1007/s00445-016-1005-8

Mutti, E., W. R. Normark., 1987, Comparing Examples of Modern and Ancient Turbidite Systems: Problems and Concepts. In Marine Clastic Sedimentology. doi:10.1007/978-94-009-3241-8_1

Németh, K., 2010, Monogenetic volcanic fields; origin, sedimentary record, and relationship with polygenetic volcanism: Special Paper Geological Society of America, https://doi.org/10.1130/2010.2470(04)

Németh, K., White, J.D.L., 2003, Reconstructing eruption processes of a Miocene monogenetic volcanic field from vent remnants: Waipiata Volcanic Field, South Island, New Zealand. Journal of Volcanology and Geothermal Research, 124(1-2): 1-21

Németh, K. and Kereszturi, G., 2015, Monogenetic volcanism: personal views and discussion. Int J Earth Sci (Geol Rundsch) 104: 2131. https://doi.org/10.1007/s00531-015-1243-6

Orton, G.J., 1996, Volcanic Environments. In Reading, H. G., 1996, Sedimentary Environments: Processes, Facies and Stratigraphy: 688 p.

Paumard, V., E. Zuckmeyer., R. Boichard., S. Jorry., J. Bourget., J. Borgomano., T. Maurin., J.-N. Ferry, 2017, Evolution of Late Oligocene - Early Miocene attached and isolated carbonate platforms in a volcanic ridge context (Maldives type), Yadana field, offshore Myanmar: 361-387 p., doi:10.1016/j.marpetgeo.2016.12.012

Planke, S., E. Alvestad, O. Eldholm., 1999, Seismic Characteristics of Basaltic Extrusive and Intrusive Rocks. The Leading Edge 18 (3): 342. https://doi.org/10.1190/1.1438289

Planke, S., P. A. Symonds, E. Alvestad, J. Skogseid., 2000, Seismic Volcanostratigraphy of Large-Volume Basaltic Extrusive Complexes on Rifted Margins. Journal of Geophysical Research 105 (B8): 19335. https://doi.org/10.1029/1999JB900005

Planke, S., T. Rasmussen, S. S. Rey, and R. Myklebust, 2005, Seismic characteristics and distribution of volcanic intrusions and hydrothermal vent complexes in the Vøring and Møre basins, in Petroleum Geology: North-West Europe and Global Perspectives – Proceedings of the 6th Petroleum Geology Conference: doi:10.1144/0060833.

Planke, S., J. M. Millett., D. Maharjan., D. A. Jerram., M. M. Abdelmalak., A. Groth., J. Hoffmann., C. Berndt., and R. Myklebust., 2017, Igneous seismic geomorphology of buried lava fields and coastal escarpments on the Vøring volcanic rifted margin: Interpretation, https://doi.org/10.1190/INT-2016-0164.1

Pope, E. L., M. Jutzeler., M. J. B. Cartigny., J. Shreeve., P. J. Talling., I. C. Wright., and R. J. Wysoczanski., 2018, Origin of spectacular fields of submarine sediment waves around volcanic islands: Earth and Planetary Science Letters, doi:10.1016/j.epsl.2018.04.020

Posamentier, H. W., V. Kolla, 2003, Seismic Geomorphology and Stratigraphy of Depositional Elements in Deep-Water Settings. Journal of Sedimentary Research 73 (3): 367–88. doi:10.1306/111302730367

Procesi, M., Ciotoli, G., Mazzini, A., Etiope, G., 2019, Sediment-hosted geothermal systems: Review and first global mapping. Earth-Science Reviews. 192. 529-544. doi:10.1016/j.earscirev.2019.03.020

Rabbel, O., O. Galland., K. Mair., I. Lecomte., K. Senger., J. B. Spacapan., R. Manceda., 2018, From field analogues to realistic seismic modelling: a case study of an oil-producing andesitic sill complex in the Neuquén Basin, Argentina: Journal of the Geological Society, doi:10.1144/jgs2017-116

Reynolds, P., N. Schofield., R. J. Brown., S. P. Holford., 2016, The architecture of submarine monogenetic volcanoes - insights from 3D seismic data: Basin Research, v. 30, p. 437–451, doi:10.1111/bre.12230

Reynolds, P., S., Holford, N. Schofield., A. Ross., 2017, Three-Dimensional Seismic Imaging of Ancient Submarine Lava Flows: An Example From the Southern Australian Margin: Geochemistry, Geophysics, Geosystems, doi:10.1002/2017GC007178

Ring, U., 2014, The East African rift system: Austrian Journal of Earth Sciences, doi:10.1016/j.jafrearsci.2005.07.019

Robertson, J., E. M. Ripley., S. J. Barnes., C. Li, 2015., Sulfur liberation from country rocks and incorporation in mafic magmas: Economic Geology, https://doi.org/10.2113/econgeo.110.4.1111

Rogers, N., 2015, Chapter 4 – The Composition and Origin of Magmas, in The Encyclopedia of Volcanoes: doi:10.1016/B978-0-12-385938-9.00004-3

Rohrman, M., 2007, Prospectivity of Volcanic Basins: Trap Delineation and Acreage de-Risking. AAPG Bulletin 91 (6): 915–39. doi:10.1306/12150606017

Rotella, M. D., C. J. N. Wilson, S. J. Barker, I. C. Wright, 2013., Highly vesicular pumice generated by buoyant detachment of magma in subaqueous volcanism: Nature Geoscience, doi:10.1038/ngeo1709

Schmiedel, T., S. Kjoberg., S. Planke., C. Magee., O. Galland., N. Schofield., C. A.-L. Jackson., and D. A. Jerram., 2017., Mechanisms of overburden deformation associated with the emplacement of the Tulipan sill, mid-Norwegian margin: Interpretation, doi:10.1190/INT-2016-0155.1

Schofield, N., L. Heaton, S. P. Holford., S. G. Archer., C. A.-L. Jackson., and D. W. Jolley., 2012, Seismic imaging of "broken bridges": linking seismic to outcrop-scale investigations of intrusive magma lobes: Journal of the Geological Society, doi:10.1144/0016-76492011-150.

Schutter, S. R., 2003, Hydrocarbon Occurrence and Exploration in and around Igneous Rocks. Geological Society, London, Special Publications 214 (1): 7–33. doi:10.1144/GSL.SP.2003.214.01.02

Senger, K., Millett, John., Planke, S., Ogata, K., Eide, C., Festøy, M., Galland, O., Jerram, D., 2017, Effects of igneous intrusions on the petroleum system: a review. First Break. 35. 47-56. 10.3997/1365-2397.2017011

Sewell, R. J., 1988, Late Miocene volcanic stratigraphy of central Banks Peninsula, Canterbury, New Zealand: p. 41–64, https://doi.org/10.1080/00288306.1988.10417809

Shumaker, L. Sharman, G., King, P., Graham, S., 2018. The source is in the sink: Deep-water deposition by a submarine volcanic arc, Taranaki Basin, New Zealand. Sedimentology. 65. 10.1111/sed.12475

Silva, S. D., J. M. Lindsay., 2015, Primary Volcanic Landforms. The Encyclopedia of Volcanoes. https://doi.org/10.1016/B978-0-12-385938-9.00015-8

Slatt, R. M., 2013, Stratigraphic Reservoir Characterization for Petroleum Geologists. Developments in Petroleum Science. doi:10.1016/B978-0-444-56365-1.00013-4

Stimac, J., F. Goff, and C. J. Goff., 2015, Intrusion-Related Geothermal Systems, in The Encyclopedia of Volcanoes: doi:10.1016/B978-0-12-385938-9.00046-8

Suggate, R.P., Stevens, G.R.,Te Punga, M.T., 1978, The geology of New Zealand. Govt Printer, Wellington.

Svensen, H., Planke, S., Malthe-Sorenssen, A., Jamtveit, B., Myklebust, R., Eidem, T.R., Rey, S.S., 2004. Release of methane from a volcanic basin as a mechanism for initial Eocene global warming. Nature 429, 542–545.

Svensen, H. H., T. H. Torsvik., S. Callegaro., L. Augland., T. H. Heimdal., D. A. Jerram., S. Planke., and E. Pereira., 2017, Gondwana Large Igneous Provinces: plate reconstructions, volcanic basins and sill volumes: Geological Society, London, Special Publications, doi:10.1144/SP463.7

Sydnes, M., Fjeldskaar, W., Løtveit, I., Grunnaleite, I., Cardozo, N., 2017. The importance of sill thickness and timing of sill emplacement on hydrocarbon maturation. Marine and Petroleum Geology. 10.1016/j.marpetgeo.2017.10.017

Thompson, N. K., K. N. Bassett., C. M. Reid., 2014, The effect of volcanism on cool-water carbonate facies during maximum inundation of Zealandia in the Waitaki–Oamaru region: New Zealand Journal of Geology and Geophysics, v. 57, no. 2, p. 149-169.

Timm, C., K. Hoernle., R. Werner., F. Hauff., P. van den Bogaard., J. White., N. Mortimer., D. Garbe-Schönberg., 2010, Temporal and geochemical evolution of the Cenozoic intraplate volcanism of Zealandia: doi:10.1016/j.earscirev.2009.10.002

Van Wagoner, J.C., Mitchum Jr., R.M., Campion, K.M., Rahmanian, V.D., 1990, Siliciclastic Sequence Stratigraphy in Well Logs, Core, and Outcrops: Concepts for High-Resolution Correlation of Time and Facies. In: American Association of Petroleum Geologists, Methods in Exploration Series 7, p. 55.

Viera de Luca, P., Matias, H., Carballo, J., Sineva, D., Pimentel, G., Tritlla, J., Cerdà, M., Loma, R., Jiménez, R. P., Pontet, M., Martinez, P. B., Veja, V., 2017, Breaking

Barriers and Paradigms in Presalt Exploration: the Pao de Açúcar Discovery (Offshore Brazil). In book: Giant Fields of the Decade 2000-2010, AAPG Memoir 113.

Wang, H. Bischoff, A.P., A. Nicol., Rossetti, M., 2018, Fluid-flow Properties of Pyroclastic Rocks – Insights from Songliao Basin, China. In 2018 Geoscience Society of New Zealand Conference, Napier, Abstract.

White, J. D. L., 1991, The depositional record of small, monogenetic volcanoes within terrestrial basins, in Sedimentation in volcanic settings. In: Sedimentation in Volcanic Settings (Eds R.V. Fisher and G.A. Smith), SEPM Spec. Publ., 45, 155–171.

White, J.D.L., 1996. Pre-emergent construction of a lacustrine basaltic volcano, Pahvant Butte, Utah (USA). Bull. Volcanol. 58, 249-262.

White, J. D. L., 2000, Subaqueous eruption-fed density currents and their deposits: Precambrian Research, 101 (2000) 87–109 https://doi.org/10.1016/S0301-9268(99)00096-0

White, J. D. L., P. S. Ross., 2011, Maar-diatreme volcanoes: A review: https://doi.org/10.1016/j.jvolgeores.2011.01.010

White, J. D. L., G. A. Valentine., 2016, Magmatic versus phreatomagmatic fragmentation: Absence of evidence is not evidence of absence: Geosphere, https://doi.org/10.1130/GES01337.1

Wight, A.W.R., Hardian, D., 1982, Importance of diagenesis in carbonate exploration and production, Lower Batu Raja Carbonates, Krisna Field, Java Sea: Indonesian Petroleum Association, 11th Annual Convention, Proceedings, p. 211–236.

Zimanowski, B., R. Büttner., V. Lorenz., H.-G. Häfele., 1997, Fragmentation of basaltic melt in the course of explosive volcanism: Journal of Geophysical Research: Solid Earth, doi:10.1029/96JB02935

Zimanowski, B., R. Büttner., 2003, Phreatomagmatic explosions in subaqueous volcanism, in Geophysical Monograph Series: doi:10.1029/140GM03